DuneFront

Deliverable 12.1

June 2025

DuneFront

Dutch Physical model of the Demonstrator(s), focus: wave-dike interactions

Deliverable 12.1 – D12.1

Deliverable information

Title	Dutch Physical model of the Demonstrator(s), focus: wave-dike interactions
Deliverable number	D12.1
WP number	12
Author(s)	Cem Sevindik, Afshar Adeli, Marion Tissier, Vincent Gruwez, Bas Hofland, Peter Troch, Oliver Lojek
Lead beneficiary	TU Delft
Contributors	UGent-E, FH, TUB
Type	Report
Dissemination level	Public
How to cite	Sevindik, Adeli, Tissier, Gruwez, Hofland, Troch, Lojek (2025) Dutch Physical model of the Demonstrator(s), focus: wave-dike interactions. DuneFront Project Deliverable 12.1, Version 1.0.
Copyright license*	

Versioning and contribution history

Version	Date	Authors (Institution)	Notes
0.01	4/06/2025	Marion Tissier (TUDelft)	Preliminary version for discussion
0.1	19/06/2025	Cem Sevindik (TU Delft), Afshar Adeli (UGent-E) and Marion Tissier (TU Delft)	Version to be checked by all WP contributors
0.6	23/06/2025	Oliver Lojek (TUB) and Vincent Gruwez (FH)	Report review
1.0	30/06/2025	All	Final version

Funded by the European Union. Views and opinions expressed are however those of the author(s) only and do not necessarily reflect those of the European Union. Neither the European Union nor the granting authority can be held responsible for them.

Funded by the European Union

DuneFront

Cover page

This report is the first deliverable of Work Package 12 (WP12 – D12.1 Dutch Physical model of the Demonstrator(s), focus: wave-dike interactions) in the DuneFront project. DuneFront focuses on better understanding dune-dike hybrid Nature-based Solutions (DD-Hybrid NbS) to create sustainable, inclusive, and aesthetic coastal management infrastructure. These innovative solutions aim to integrate biodiversity while addressing significant socio-economic challenges along Europe's densely populated coasts.

The primary objective of Work Package (WP) 12 is to evaluate the coastal protection functioning of DD-hybrid NbS during extreme storms. This requires gaining new insights into the physical processes specific to storm wave interactions with DD-hybrid NbS, such as dune erosion in the presence of a hard structure, the effect of the eroding dune on wave transformation, dike loading, wave overtopping, and wave impacts, but also dune strengthening by vegetation. To obtain those, currently unavailable data on the functioning of DD-Hybrid NbS under extreme storm conditions will be collected using dedicated physical experiments of a selection of the DuneFront demonstrators. The physical modeling data will be used to validate and improve the process-based numerical models and subsequently expand the physical model dataset for a wider range of conditions and geometries of the DD-Hybrid NbS.

The present report describes the first experimental campaign of WP12. In the scope of this task (D12.1), TU Delft has realized the physical modeling campaign by considering different demonstrators from the project in the wave flume in close collaboration with UGent-E and FH. The main objective of this task is to provide a database of wave hydrodynamics, wave overtopping, and wave loads on the dike after dune erosion by focusing on the hydrodynamics. To fulfill this objective, different bed profiles representing the demonstrators after erosion during extreme storm conditions and water levels were considered. During the experiments, three different types of wave sets, which are irregular, bichromatic, and bimodal, were generated in the wave flume to further understand the performance of the tested model under different wave conditions. A total of 168 wave sets (test runs) were performed in the physical model. Wave gauges and ultrasonic sensors were used to measure water surface elevation and wave overtopping. Piezoresistive-type pressure sensors were placed to measure the wave impact pressures on the dike model, and electromagnetic flow meters were installed to record flow velocity along the wave flume. Lastly, PIV was used for selected tests to capture the overtopping-flow velocities on the dike.

In the present report, the schematization of the studied demonstrators is explained, and the experimental setup and the test program are described in detail. Furthermore, some examples of the data post-processing and first visualizations of the gathered experimental data are presented. Finally, the dataset archiving structure is described.

DuneFront

Table of Content

Notation

Parameter	Explanation
α_{beach}	Beach slope (degrees)
α_{berm}	Slope of the foreshore (berm) that forms in front of the dike after dune erosion (degrees)
α_{dike}	Seaward dike slope (degrees)
h_{deep}	Depth at which the offshore wave boundary conditions are specified (m)
h_{toe}	Depth at toe of the dike after dune erosion (m)
H_{m0}	(Spectral) significant wave height (m)
$H_{m0,IG}$	Offshore significant wave height for free infragravity waves (m)
$H_{m0,,ss}$	Offshore significant wave height for sea-swell waves (m)
$R_{c,dike}$	Dike crest freeboard relative to extreme/design water level (m)
$T_{p,ss}$	Peak wave period for the sea-swell waves (s)
$T_{p,IG}$	Peak period for the infragravity waves (s)
W_{dike}	Crest width of dike (m)

List of abbreviations

Abbreviation	Explanation
BE	Belgium
DD	Dune-Dike
DD-Hybrid	Dune-Dike Hybrid
EMF	Electromagnetic Flow meter
FIG	Free infragravity waves
IG waves	Infragravity waves
MIC	Mic Ultrasonic Sensor
MSL	Mean sea level
NbS	Nature-based Solution
NL	The Netherlands
WG	Wave Gauge
WP	Work Package

1. Introduction

1.1 General background

The primary objective of the DuneFront project is to optimize dune-dike hybrid Nature-based Solutions (DD-Hybrid NbS) as a new generation of sustainable, nature-inclusive coastal protection. Such coastal protection measures, that combine a hard safety line (dike) and biodiverse and resilient dune systems, have the potential to adapt to sea-level rise provided that the physical and biological conditions are met. In this context, a key challenge of DuneFront is to identify the biological, physical, and socio-economic boundary conditions and their interactions to enhance the protection provided by these hybrid approaches. The DuneFront concept is summarized in Figure 1.

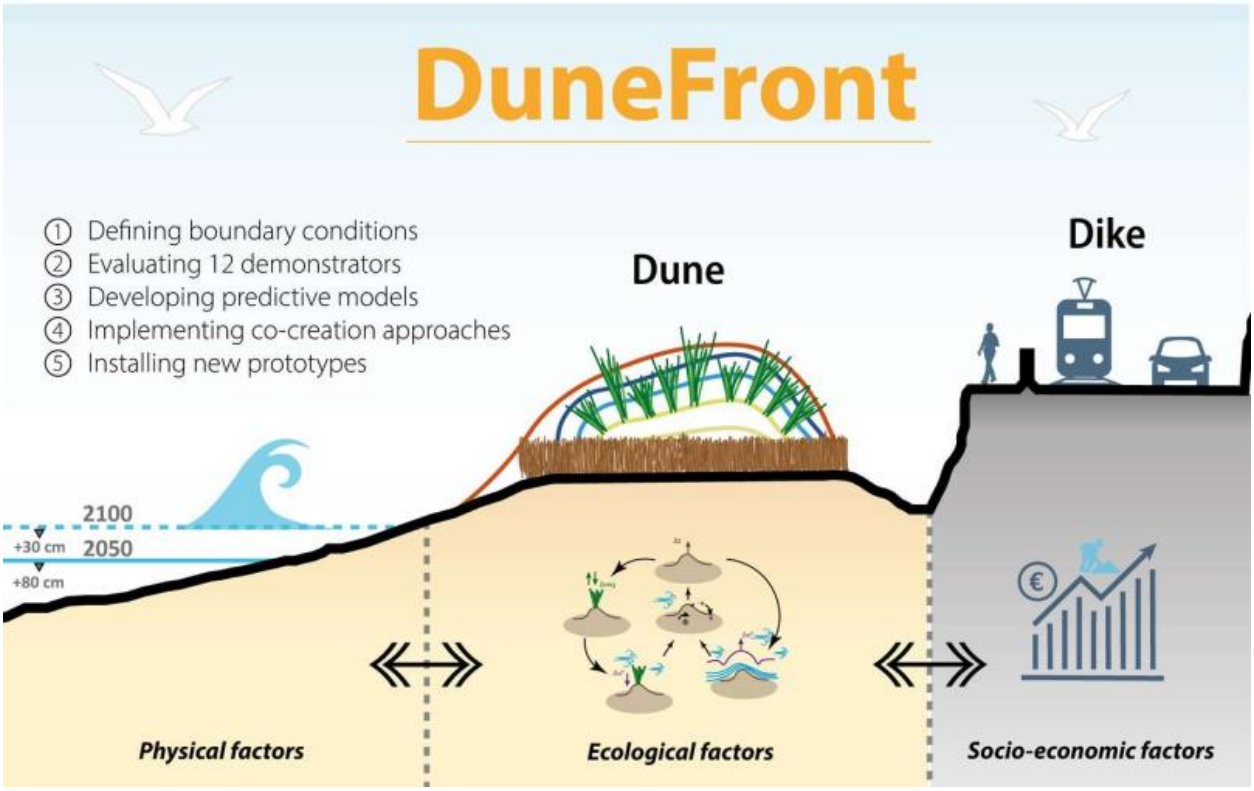

Figure 1 - DuneFront concept in one graphical abstract

1.2 Overview of Work Package 12

1.2.1 Work Package description

The primary objective of Work Package (WP) 12 is to evaluate the coastal protection functioning of DD-hybrid NbS during extreme storms. This requires gaining new insights into the physical processes specific to storm wave interactions with DD-hybrid NbS, such as dune erosion in the presence of a hard structure, the effect of the eroding dune on dike loading,

wave overtopping, and wave impacts, but also dune strengthening by vegetation. To obtain those, currently unavailable data on the functioning of DD-Hybrid NbS under extreme storm conditions will be collected using dedicated physical experiments of a selection of the DuneFront demonstrators, using the input from WP7. These so-called Physical Twins will also be used to communicate with stakeholders (WP17). The physical modeling data will be used to validate and improve the process-based numerical models and subsequently expand the physical model dataset for a wider range of conditions and geometries of the DD-Hybrid NbS. Ultimately, this will be used to demonstrate the efficiency of the DD-Hybrid NbS coastal protection system as an adaptive defense against climate change impacts.

1.2.2 Work Package sub-tasks and deliverables

WP12 consists of 5 tasks listed below, each of them associated with a deliverable:

Task 12.1. Physical modeling of the Dutch Demonstrator(s), focus: wave-dike interactions (Deliverable D12.1, this report)

Task 12.2. Physical modeling of the German Demonstrator(s), focus: vegetation influence on dune erosion (Deliverable D12.2, March 2026)

Task 12.3. Physical modeling of the Belgian Demonstrator(s), focus: dune-dike interactions (Deliverable D12.3, September 2026)

Task 12.4. Validation of the numerical models XBeach-SB, XBeach-NH, and SWASH using the experimental data (Deliverable D12.4, December 2025)

Task 12.5. Demonstration of the DD-hybrid NbS coastal protection efficiency using the validated models (Deliverable D12.5, June 2027)

1.3 Aims of D12.1

In the scope of D12.1 (this report), TU Delft has realized the physical model for the Dutch Demonstrator in the wave flume in close collaboration with UGENT-E and FH. The main objective of this task is to provide a database of wave hydrodynamics, wave overtopping and wave loads on the dike after dune erosion by focusing measurements on the hydrodynamics.

1.4 Outline of this report

This report is structured as follows: Section 2 describes the schematization process of the demonstrators for the laboratory experiments, building on the work performed in WP7. Section 3 presents the experimental setup. The test program followed during the experiments is presented in Section 4. Then, in Section 5, data processing is discussed and some first visualizations of the gathered data are provided. Finally, the dataset structure and archiving are discussed in Section 6.

2. The experiments as physical twins – Schematization of the demonstrators

The Dutch experiments, focusing on dike processes, were the first physical modelling campaign carried out in the scope of WP12. The focus of these experiments was on the hydrodynamics at (or slightly after) the peak of the design storm, where the dike is revealed following dune erosion and the eroded sand is deposited in front of the dike, creating a berm that forms a shallow foreshore. Fixed beds were used to represent both the sandy and hard parts of the hybrid system after erosion. All configurations considered in the experiments were designed according to the geometric schematization presented in DuneFront deliverable D7.2. (see Figure 1).

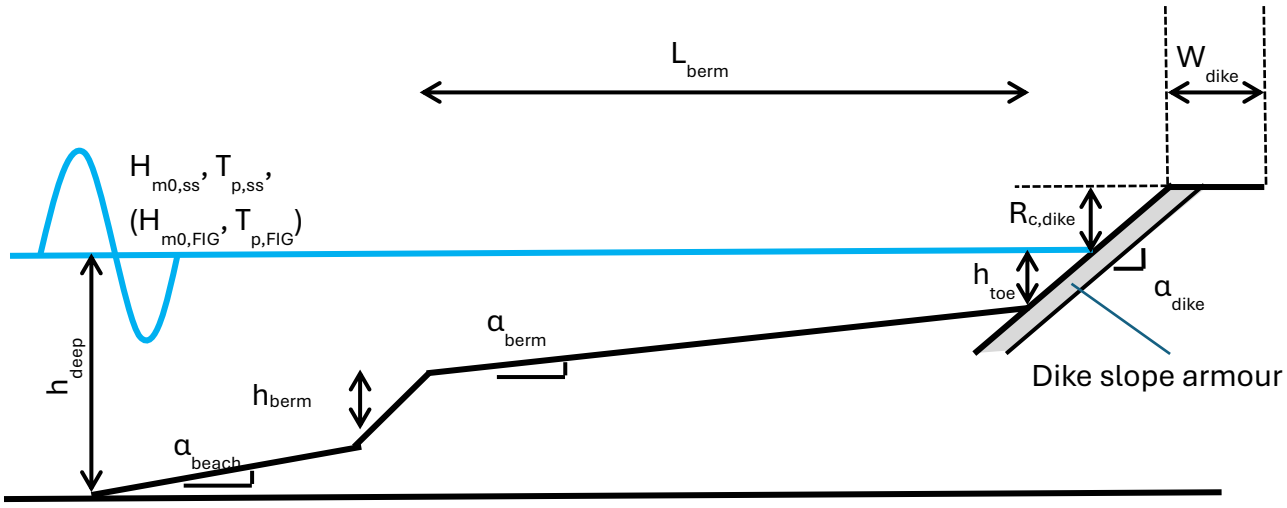

Figure 1 - General setup for physical model test series on dike processes; These tests focus on the wave-dike interactions after dune erosion, where the wave loads on the dike are expected to be (near) maximum. Sand deposition following dune erosion is schematized by a berm of height h_{berm} and length L_{berm}, decreasing the bed slope and the depth in front of the dike. Adapted from Sevindik et al., 2024 (D7.2)

The experimental set-up was designed to be representative of the Katwijk (NL) and Raversijde (BE) demonstrators. The bed geometry and hydraulic conditions were chosen to resemble as much as possible the conditions expected at these demonstrators around the peak of the design storm while accounting for practical constraints. These considerations resulted in the test ranges presented in Table 1 (last column, at prototype scale). In this table, these actual test ranges are compared to the expected conditions at Katwijk and Raversijde (first two columns), as determined in WP7. The main schematization choices and compromises are discussed below.

The analysis carried out in WP7 revealed that the beach slope at the selected demonstrators (α_{beach}) varied between 1/35 and 1/50, while the berm slope (α_{berm}) varied between 1/45 and

1/60, with in general milder slopes for Raversijde than for Katwijk (see Table 1). To minimize variations in the bed profile, a representative beach slope of 1/40 and a representative foreshore of 1/50 were chosen to represent both Katwijk and Raversijde. Two berm lengths (L_{berm}) were however used to account for differences in initial dune volume at both demonstrators, which result in different volumes of deposited sand after erosion (see details in Section 3.2). Furthermore, one unique dike design was considered for both experiments: a smooth dike slope of 1/3.

Due to practical constraints (e.g., flume dimension and scaling, limiting the maximum offshore water depth d_{deep}), the maximum significant wave height $\mathbf{H_{m0,ss}}$ considered was only 4 m, which is significantly less than the expected 8 m significant wave height for the design storm at Katwijk, but is close to the design storm wave height for Raversijde. Smaller $H_{m0,ss}$ were also considered in the experiment as a way to (partly) compensate for the overestimation of the bound IG wave energy by the long-crested waves that are generated in the wave flumes (compared to the bound IG of short-crested waves in the field).

When the Demonstrators were designed, the presence of offshore generated free infragravity (FIG) waves was not taken into account. It has been found recently that significant amounts of FIG waves can also be present in the North Sea (Reniers et al., 2021; Rijnsdorp et al., 2021, and more recently Akrish et al., 2025). In the tests, the potential effect of these FIG was examined. While most tests were performed without these additional FIG, several tests were repeated with the addition of very large offshore free IG waves $H_{m0,FIG}/H_{m0,ss} \approx 0.19$–$0.38$.

*Table 1 - **Prototype scale** test ranges considered in the Dutch physical model test on dike processes compared to the ranges defined in the framework of WP7 (Sevindik et al., 2024; D7.2) for Katwijk (NL) and Raversijde (BE).*

Hydraulic parameters	Schematization of Katwijk (NL) from D7.2	Schematization of Raversijde (BE) from D7.2	Prototype scale test ranges for dike experiments
$H_{m0,ss}$ (m)	8	4.7	2 to 4
$T_{p,ss}$ (s)	13.9	9.9	8 to 14
$H_{m0,FIG}$ (m)	-	-	0.75
$T_{p,FIG}$ (s)	-	-	44 and 66
h_{deep} (m)	25.30	12.37	16.30 to 18.45
Dike parameters			
W_{dike} (m)	15	6.30	10
Rc_{dike} (m)	1.3 to 2	2.85	1.1 to 3.25
cot α_{dike} (-)	3	2	3
h_{toe} (m)	1 to 2	0 to 1	1.25, 2 and 2.5
Berm and beach parameters			
L_{berm} (m)	≈ 300	≈ 200	200 and 300 (two profiles considered)
h_{berm} (m)	1 to 2	2.5	0, 2.25 and 2.75
cot α_{berm}	45 to 50	60	50
cot α_{beach}	35 to 41	30 to 50	40

3. Experimental setup

3.1 Experimental facilities

The laboratory experiments were conducted in the wave flume of the Hydraulic Engineering Laboratory at Delft University of Technology, Delft, The Netherlands, from April to June 2025. The flume is 39 m long, 0.79 m wide, and 1 m high; it has glass windows along most of its length (Figure 2). The waves were generated with a piston-type wave maker with 2 m stroke, and equipped with Active Reflection Compensation (ARC) to minimize reflections from the wave paddle.

Figure 2 – Wave flume during the experiments at TU Delft (photo taken during the stakeholder visit on April 25, 2025 by Line Debaveye)

3.2 Bed profile configurations

Model setups were designed with a **1/25 Froude-type length scale**. In total, 6 configurations of the bed profile were considered, in two successive phases. The bed profiles were made of plywood.

In **Phase 1** of the experiment, three main bed profiles were successively considered:

- The first profile corresponds to the dike-only case, called 'Base Case' in the following. Here a dike is installed directly at the end of a 1/40 planar beach (Figure 3a). It can be used as a reference to evaluate the protection provided by the berm that forms after dune erosion. Moreover, it links to earlier studies on linear slopes.
- The second and third profiles correspond to the eroded dune-dike situation, where an additional step of slope 1/50 is installed offshore of the dike on top of the main 1/40 beach slope to represent the sand deposited in front of the dike after dune erosion.
    - The second profile schematizes the eroded profile of the Raversijde demonstrator, with a step length of 8 m (Figure 3b).
    - The third profile schematizes the eroded profile of the Katwijk demonstrator, with a longer step (+4 m) because of the larger original dune volume (Figure 3c).

In **Phase 2** of the experiment, the same bed profiles are considered, but now without the dike. More specifically, the dike is removed and replaced with a gentle porous slope consisting of

rocks of approximately 5 cm in diameter to act as a wave absorber. With the wave absorbers in Phase 2, it is aimed to quantify the incoming wave conditions to characterize wave loads and overtopping at the dike. A drawing of the setup for Phase 2 is given in Figure 4 for the three profiles considered. Also, photographs presenting the dike section and the stone section after removing the dike are presented in Figure 5.

The beach profile was built in such a way that it allows water to seep through its base (around x=8 m) connecting the water body behind the dike to the offshore part and ensuring that overtopping over the dike does not lead to a significant loss of water on the offshore part. Only the water captured by the overtopping chute is stored in the overtopping tank and "lost" during a test (see Section 3.3 for more explanations).

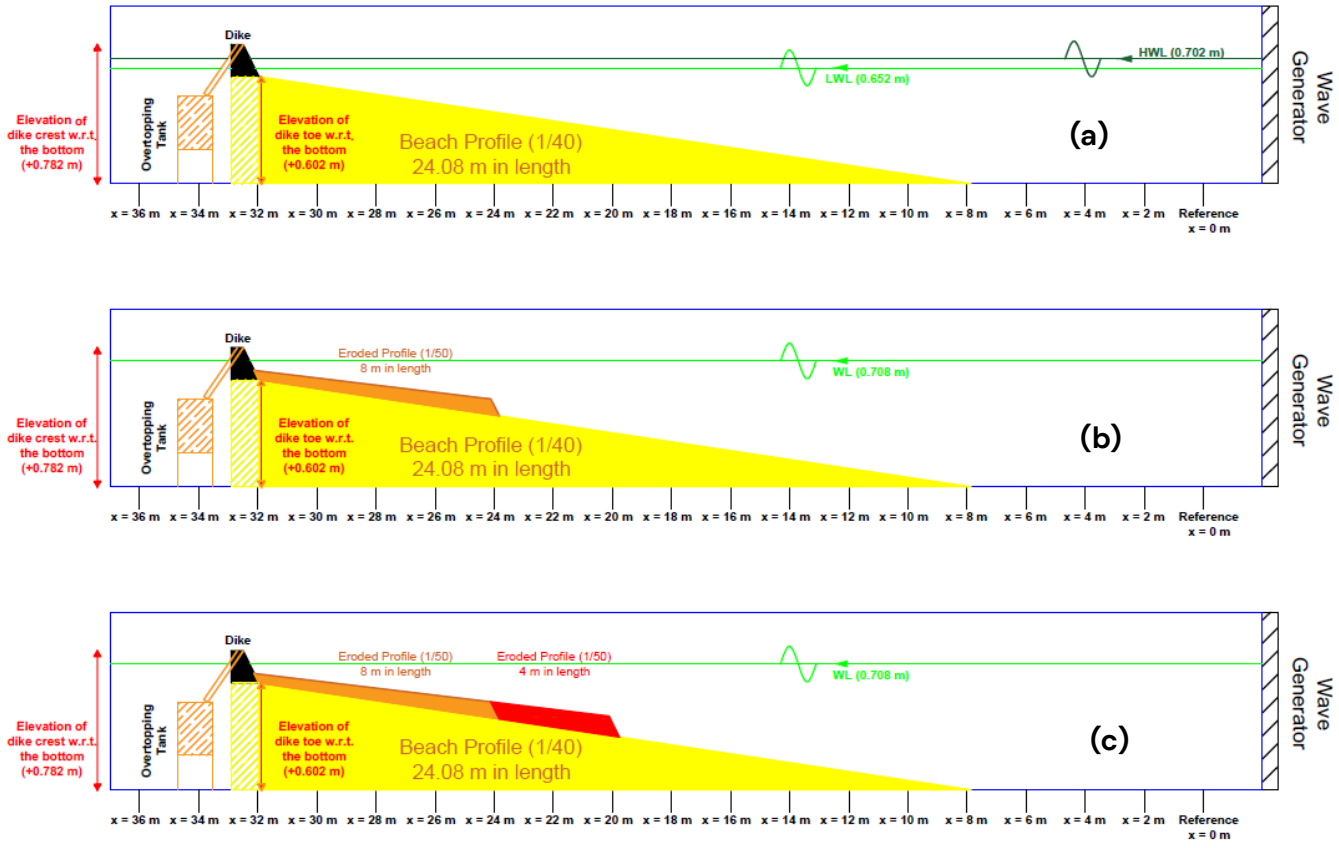

Figure 3 – Bed profiles for Phase 1 of the experiments with (a) the dike-only base case, (b) the "Raversijde" eroded profile, and (c) the "Katwijk" eroded profile

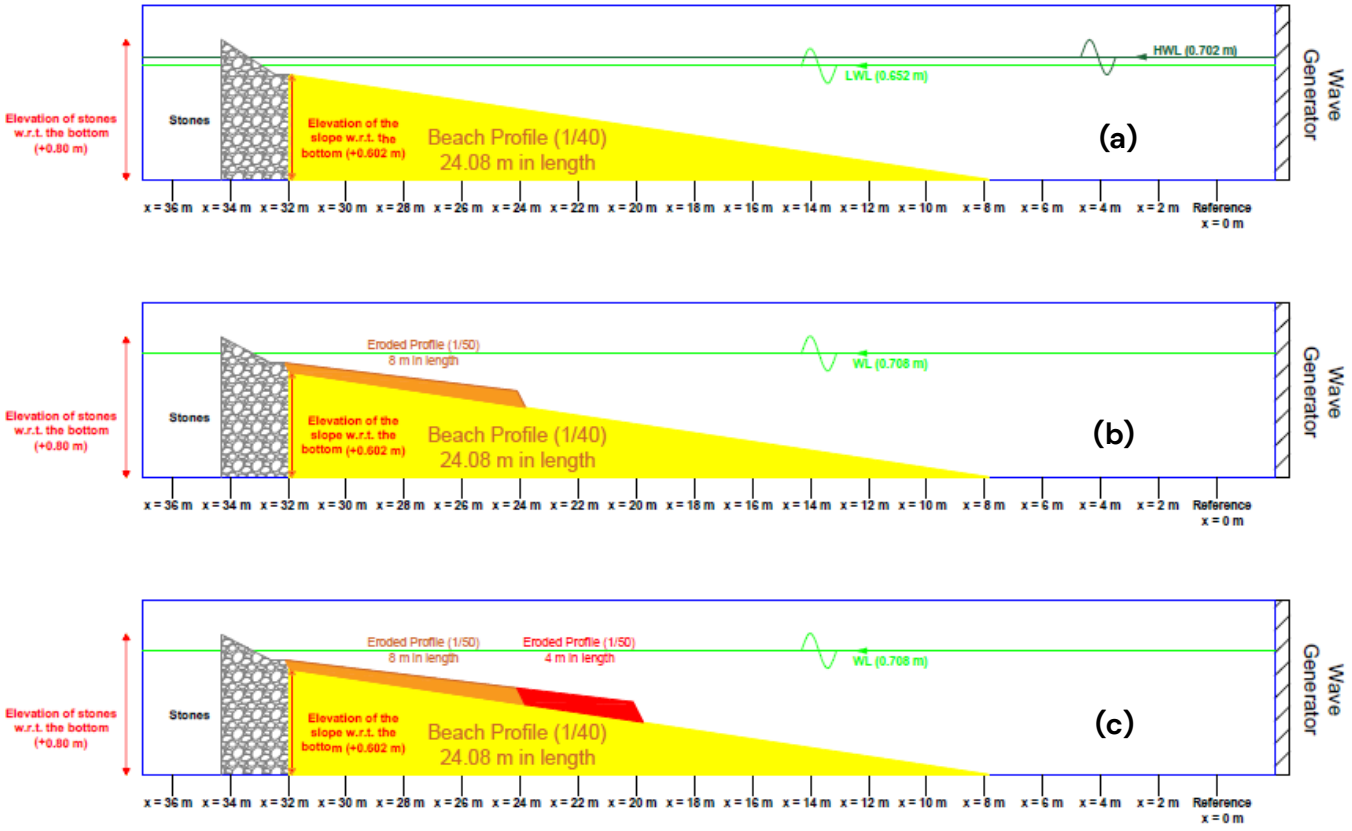

Figure 4 – Bed profiles for Phase 2 of the experiments with (a) the dike-only base case, (b) the "Raversijde" eroded profile, and (c) the "Katwijk" eroded profile

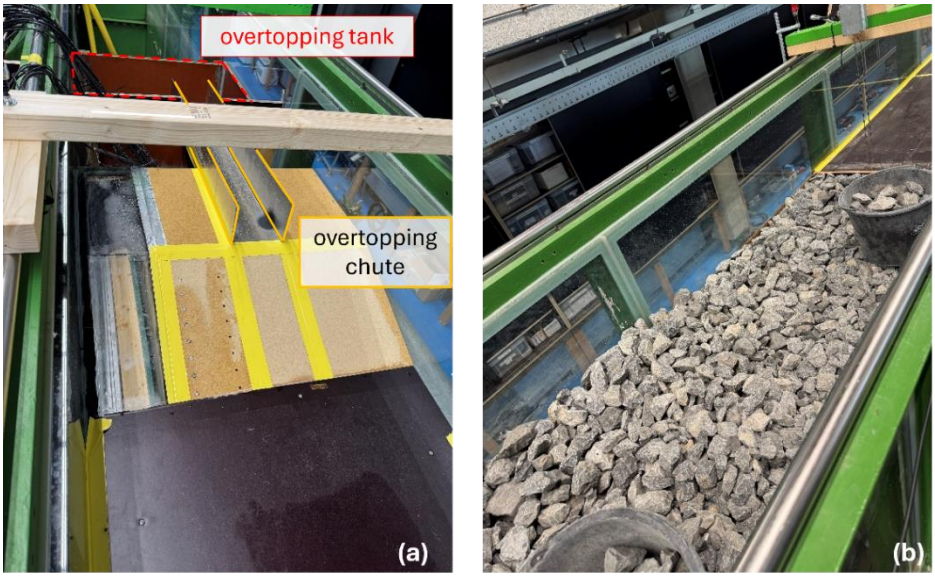

Figure 5 – (a) Constructed dike section for Phase 1 (with in black the foreshore berm), including an overtopping chute connecting the dike crest to the overtopping tank, and (b) located stones after removing the dike structure for Phase 2.

3.3 Dike and overtopping tank

Figure 6 presents the design of the dike used in Phase 1 of the experiments. The dike had a height of 18 cm from toe to crest and a horizontal crest section of 40 cm in along-flume direction. The first 18 cm of the dike section, measured from the flume wall in the cross-flume direction, were made transparent using Plexiglas to allow for PIV measurements (see Section 3.4.3 for more details).

An overtopping tank of inner dimensions 45 cm in height, 75 cm in cross-flume direction, and 80 cm in along-flume direction was installed behind the dike during Phase 1 of the experiment. The dimensions of the overtopping box were determined based on preliminary numerical simulations using XBeach (Roelvink et al., 2009) which were used to estimate overtopping volumes. The overtopping tank was connected to the outer dike crest by a downward sloping chute (see position of the chute on the dike in Figure 6).

The overtopping chute had a width of 15 cm in cross-flume direction, representing 19% of the total dike crest length. It was made of stainless steel, with vertical side screens of height 15 cm and thickness of 2 mm (see picture in Figure 5a). This relatively narrow overtopping chute was designed to minimize the volume of water "captured" by the overtopping tank during a test series, as this volume is effectively lost from the main water body, ultimately leading to a lowering of the offshore water level. A maximum decay in the still water level of 3 mm was observed between the start and the end of the test for the most extreme conditions, which was deemed acceptable. In general, observed decays in the water level ranged between 1 and 3 mm for irregular and bimodal wave sets. During the bichromatic wave sets that have relatively shorter durations of 10 minutes, water level decays were negligible (less than 1 mm).

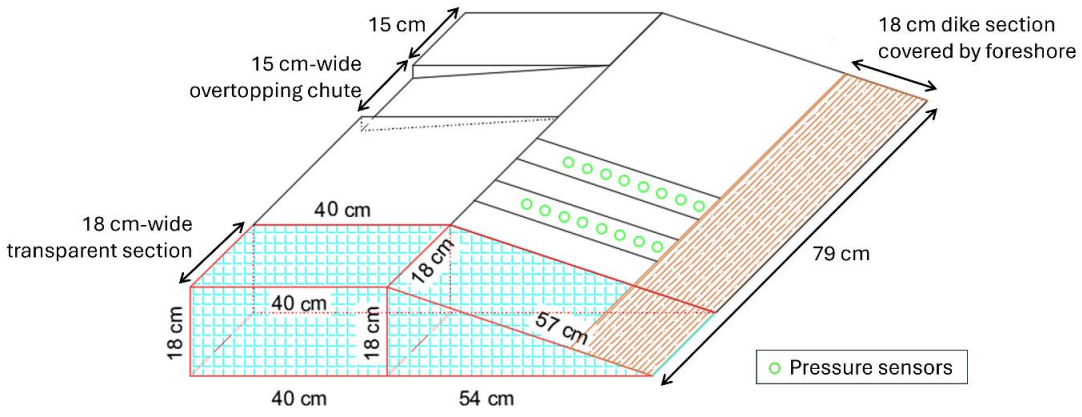

Figure 6 – Design of the dike for Phase 1 of the experiments. The area in brown is the section of the dike that is covered by the foreshore berm when considering the Katwijk and Raversijde profiles (Fig. 3b and 3c). The area in blue was built out of Plexiglas and was thus transparent (needed for PIV measurements, see Section 3.4.3). The positioning of the pressure sensors, described in Section 3.4.2, is shown by the green circles (8 Kulites sensors on the left side and 8 Honeywell sensors on the right side).

3.4 Instrumentation

During the experiments, several measurement devices were used for different purposes. During Phase 1 of the experiments:

- 15 resistance-type wave gauges were used to measure the water surface elevation under wave action. One of these sensors was located inside the wave overtopping box to record the water elevation increase for the overtopping measurements.
- 3 ultrasonic sensors were used to measure the water elevation. Two of these sensors were placed on the crest part of the dike section to detect flow thicknesses and characterize individual overtopping events, and one of them was located inside the wave overtopping box to record the water elevation increase for the overtopping measurements.
- 9 electromagnetic flow meters were used to measure horizontal flow velocity in the direction of the propagating waves.
- 16 pressure sensors to measure the wave impact pressures on the front face of the dike section.
- An LED-PIV system, including a camera and LED-light sheet, to measure the particle velocities during overtopping for the bichromatic wave sets on the Katwijk configuration.

During Phase 2 of the experiments,

- 14 wave gauges were used to measure the water surface elevation under wave action.
- 9 electromagnetic flow meters were used to measure horizontal flow velocity in the direction of the propagating waves.

For both phases, except for the LED-PIV system, all instruments were synchronized, and the data was sampled at 500 Hz.

3.4.1 Wave measurements

In total, 15 wave gauges (WG) and 9 electromagnetic flow meters (EMF) were installed at measuring stations along the flume. These were collocated along the flume so as they can be used to separate incoming and reflected wave components (e.g., Guza et al., 1984; Buckley et al., 2015). Five wave gauges were furthermore deployed in an array on the horizontal part offshore of the slope to follow the wave reflection analysis methodology proposed by Eldrup and Andersen (2019).

Below, in Figure 7 and Figure 8, the placement of the measurement devices, except the LED-PIV system, is presented for Phase 1 and Phase 2, respectively. In these figures, the reference point (x = 0 m) is 2 m in front of the zero position of the piston of the wave generator. In Annex A – Positions of the wave gauges and electromagnetic flow metersthe precise positions of

the wave gauges and electromagnetic flow meters are given for all bed profiles, for both Phase 1 and Phase 2.

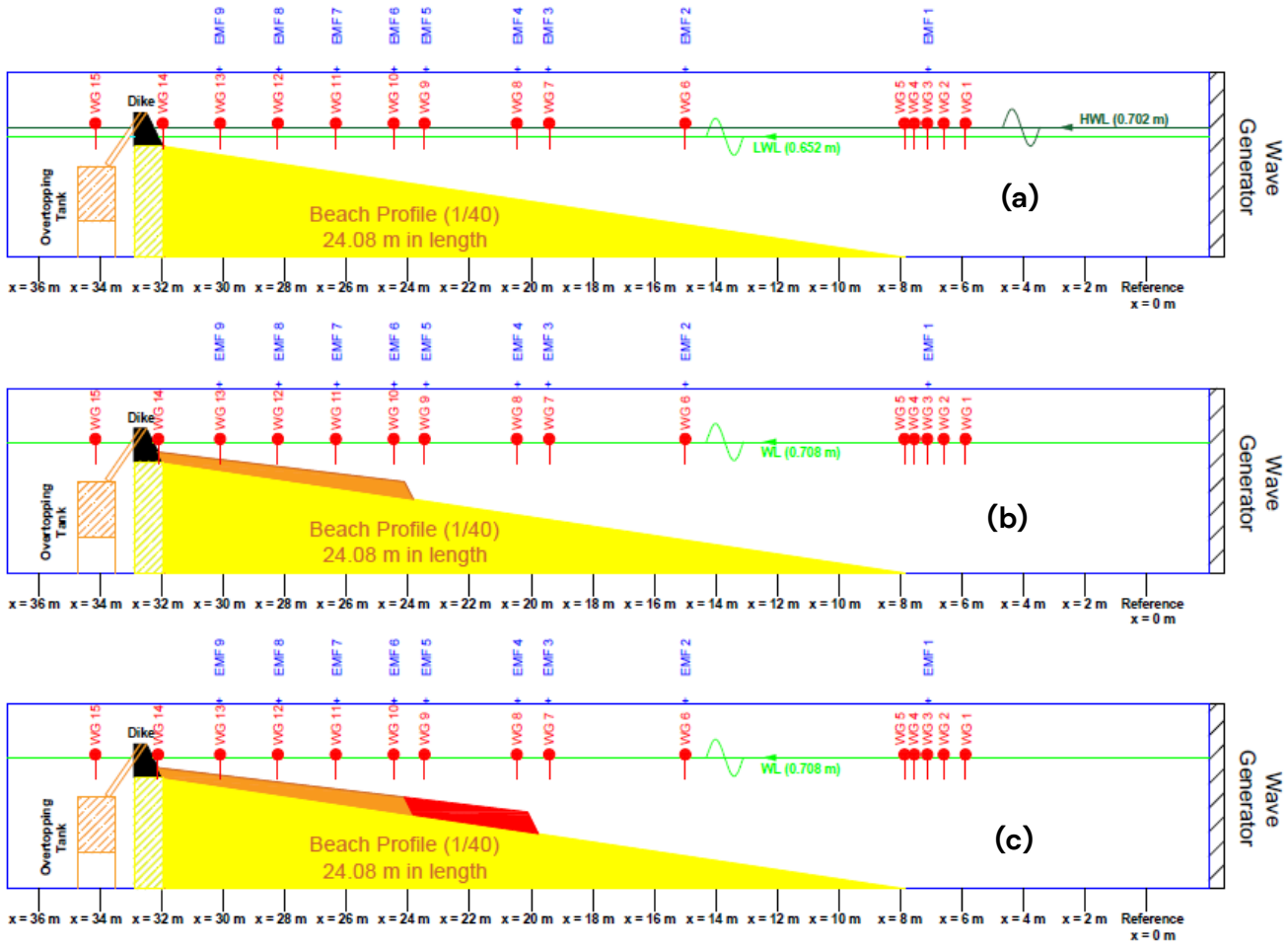

Figure 7 – Positions of WGs and EMFs for Phase 1 of the experiments with (a) the base case (dike-only), (b) the Raversijde eroded profile, and (c) the Katwijk eroded profile.

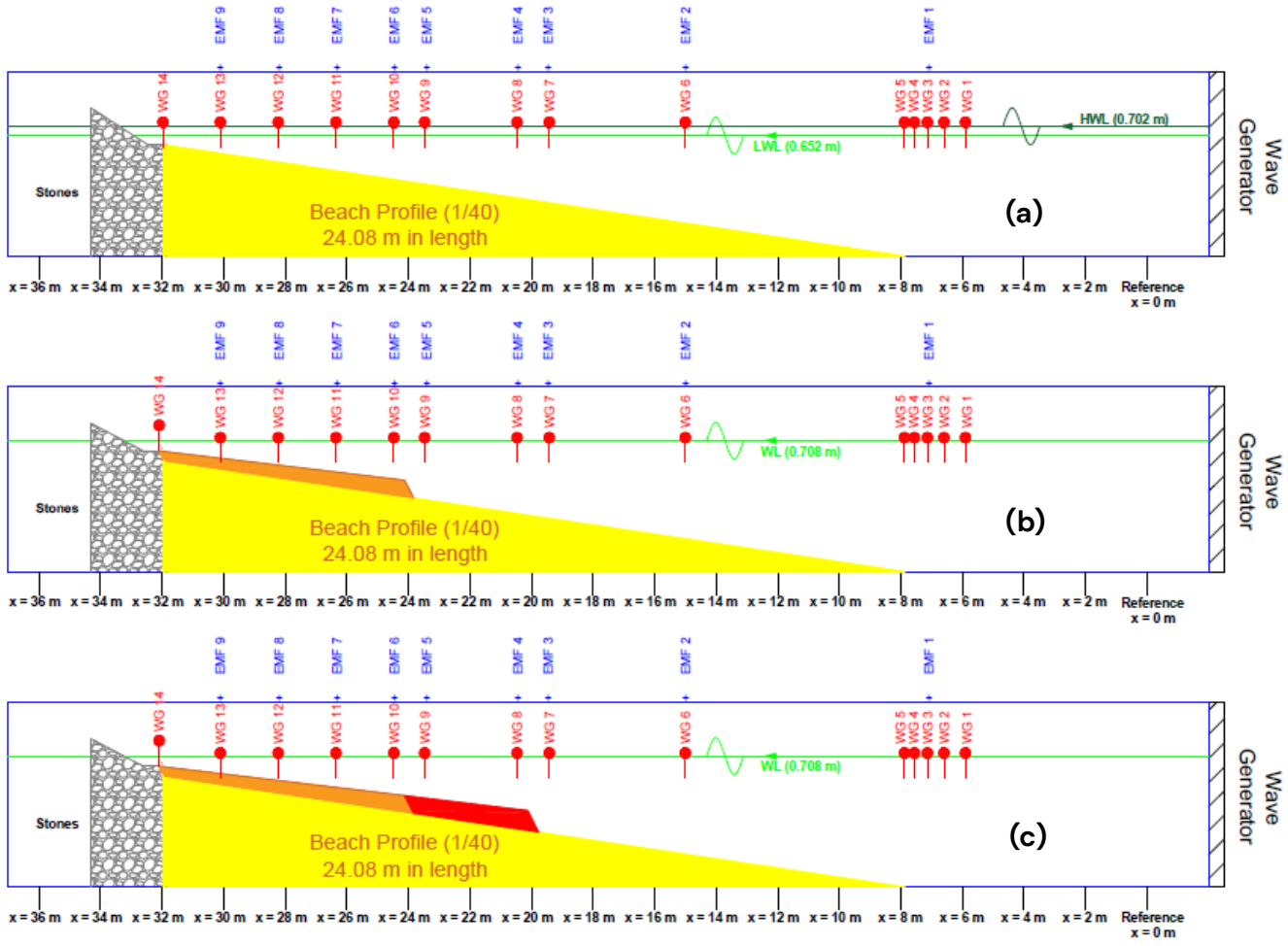

Figure 8 - Positions of WGs and EMFs for Phase 2 of the experiments with (a) the base case (dike-only), (b) the Raversijde eroded profile, and (c) the Katwijk eroded profile.

3.4.2 Wave impact on the dike

For the wave impact pressure measurements on the dike section, a total of 16 pressure sensors in 2 different types were used. These two types are:

- Kulite HKM-375 piezoresistive type miniature threaded pressure transducer (8 mm diameter membrane flush to the slope)
- Honeywell 24PC piezoresistive type miniature pressure transducer (1.2 mm diameter pinhole in the slope, filled with water).

These pressure sensors were placed in two vertical lines (one line per sensor type, see green circles in Figure 6) along the front dike slope. The precise positioning and spacing of the pressure sensors on the dike structure's front face is given in Figure 9. A 4 cm distance was left between the centers of successive sensors along a line. The center of the upper sensors of each line were located at a distance (measured along the dike front slope) of 9 cm from the top of the dike structure. The centers of the lower pressure sensors of each line were positioned 20 cm from the toe of the dike.

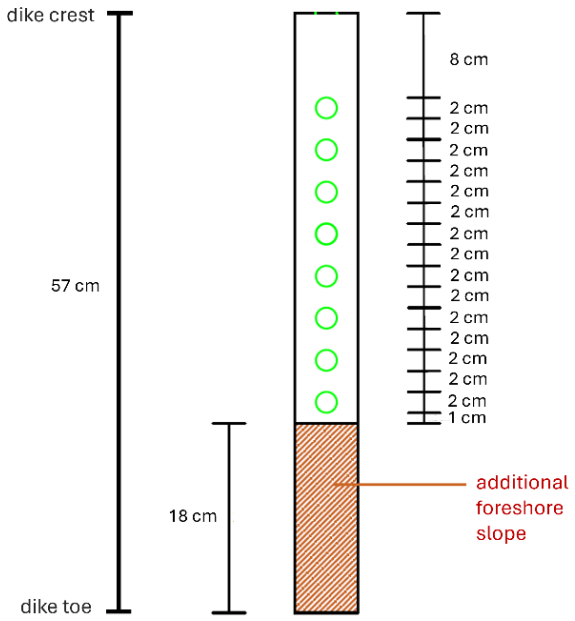

Figure 9 - Positioning of the pressure sensors along the dike slope (green circles). Kulite and Honeywell sensors were installed with the same spacing. See Figure 6 for a view of the entire dike, including the two lines of pressure sensors. The brown part indicates the lower section of the dike slope that is covered by the additional slope (berm) during the experiments with the Raversijde and Katwijk profiles.

3.4.3 Characterization of overtopping events

In addition to the single wave gauge inside the wave overtopping box, 3 mic+25/IU/TC type ultrasonic sensors with one analogue output were used for the wave overtopping measurements. These sensors measure the distance between the sensor and the first detected interface, which is either the water surface or the bed, depending on the time and location. Two of these sensors were placed on the crest part of the dike section to detect flow thicknesses, and one of them was located inside the wave overtopping box alongside the wave gauge to record the water elevation increase after each wave overtopping event. In the post-processing of the data, flow velocity will be calculated by the time difference between the passage of wave fronts detected from MIC1 and MIC2, after individual wave overtopping events. The positioning of the 3 ultrasonic sensors (MIC 1 to MIC 3) is presented in Figure 10.

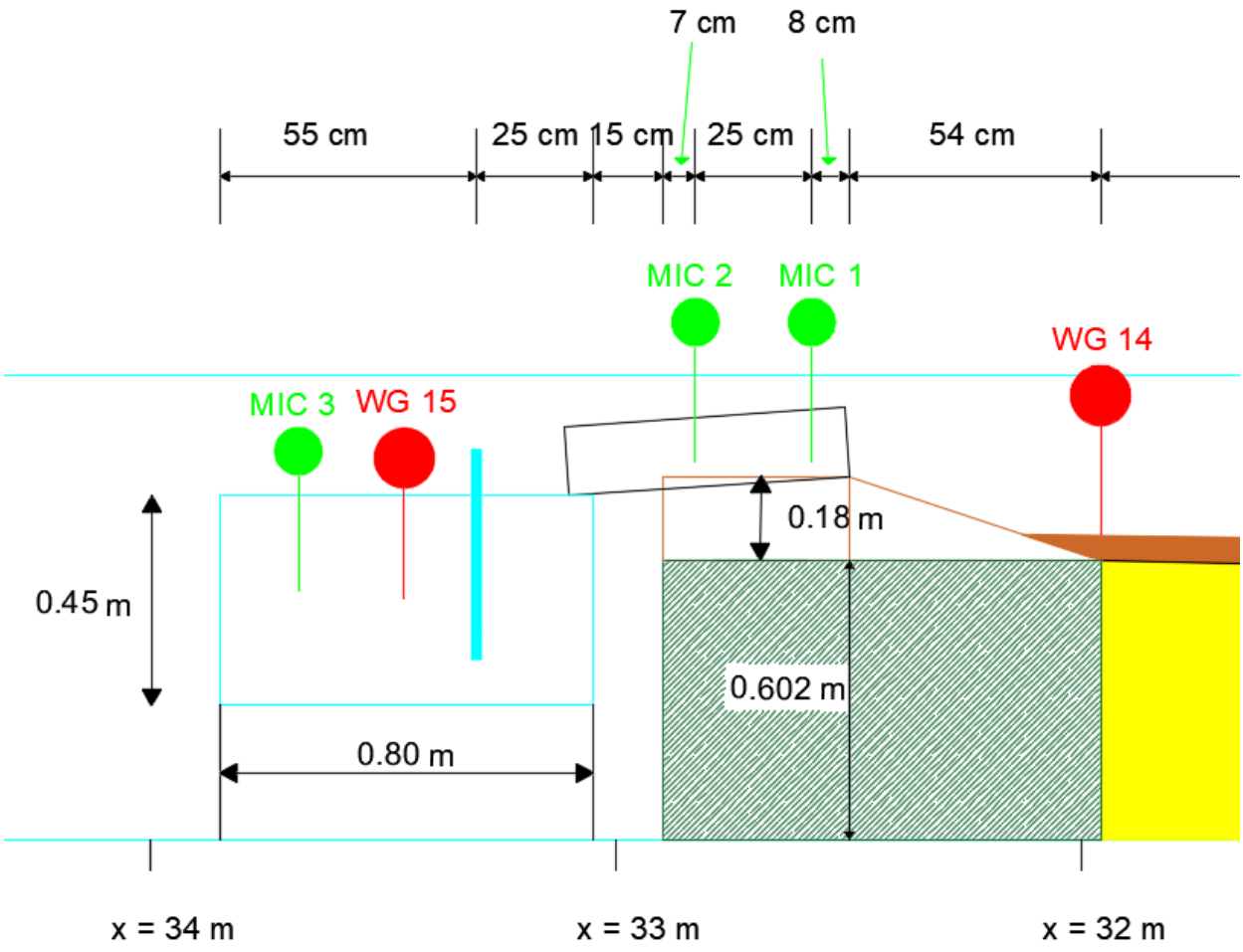

Figure 10 – Positioning of the three ultrasonic sensors (green dots), MIC 1-3 for Phase 1.

For the Katwijk slope in Phase 1, the **LED-PIV system** was used to record the particle velocities and flow layer thicknesses for bichromatic wave sets for individual wave overtopping

measurements. This system consists of a camera, a horizontal LED light sheet, and a horizontal mirror, 75 cm in length. The LED-PIV system is described in Bakker et al. (2021).

To use this system, a transparent section made of plexiglass material with an 18 cm width was designed for the dike part of the setup in Phase 1 (blue shaded area in Figure 6). Inside this transparent part, a mirror was placed at a 45-degree angle to reflect the lights produced by the horizontal LED light sheet device of the system so as it could shine vertically through the dike structure and illuminate the water during overtopping events. A photograph of the system is given in Figure 11, including the horizontal light sheet, camera, transparent part and the mirror.

To measure the velocities, small white particles (seeding, with diameter of 100 micron, and density of 1060 kg/m^3) were added to the water near the dike section during the experiments, and the motion of these particles was recorded by the camera. 2-minute-long camera recordings were taken for each bichromatic wave set in Phase 1 for the Katwijk bed profile. A 50 Hz sampling frequency was applied for these recordings.

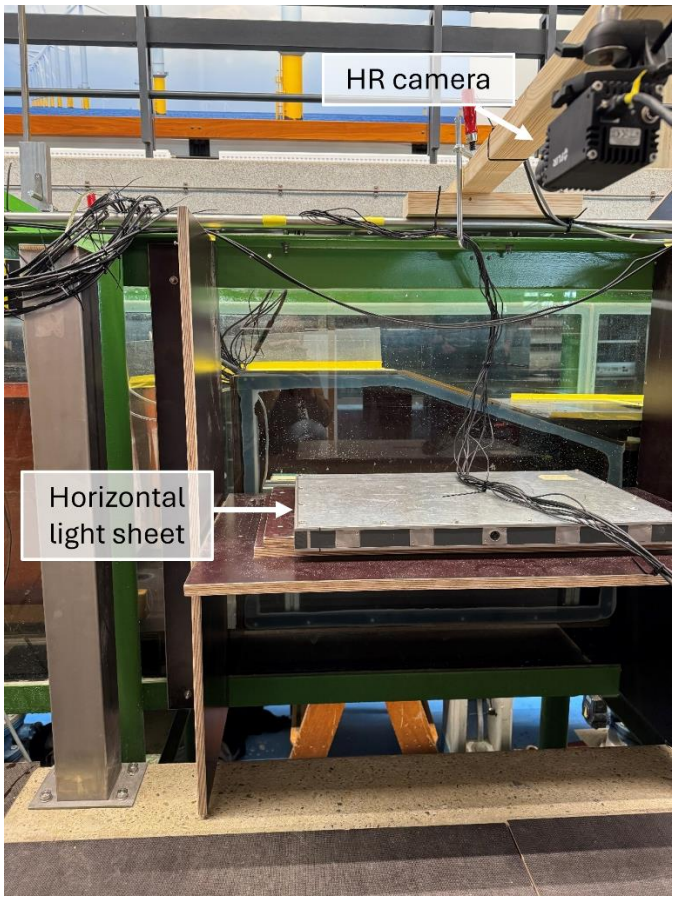

Figure 11 – The LED-PIV system for overtopping measurements next to the transparent dike section.

4. Test program

A total of 84 wave conditions were run, grouped in 3 test series with varying complexity. These groups are irregular wave sets (**test series A**), bichromatic wave sets (**test series B**), and bimodal irregular wave sets (**test series C**). All wave-paddle steering signals were made with second-order wave generation. All 84 wave sets were repeated in Phase 2 of the experiments, after removing the dike section and filling the backside of the setup with stones to construct a passive absorption system for long waves. Details on the naming of the wave sets are given in Section 6.

In **test series A** (Table 2, Table 3 and Table 4), the signals were based on a JONSWAP spectrum with a peak enhancement factor γ of 3.3. Peak periods varied between 1.6 s and 2.8 s, while the significant wave height varied between 0.08 m and 0.16 m. Two water levels were furthermore considered.

Table 2 – Test series A (irregular wave sets) for base (reference) case (BC) configuration; $H_{m0,ss}$ and $T_{p,ss}$ are the target significant wave heights and periods for the Jonswap spectra.

Wave Set	Water depth at paddle (m)	Duration (min)	Number of Waves	$H_{m0,ss}$ (m)	$T_{p,ss}$ (s)
BC_652_IR_8_16	0.652	45	≈2000	0.08	1.6
BC_652_IR_8_22	0.652	62	≈2000	0.08	2.2
BC_652_IR_8_28	0.652	78	≈2000	0.08	2.8
BC_652_IR_12_16	0.652	45	≈2000	0.12	1.6
BC_652_IR_12_22	0.652	62	≈2000	0.12	2.2
BC_652_IR_12_28	0.652	78	≈2000	0.12	2.8
BC_652_IR_16_16	0.652	23	≈ 1000	0.16	1.6
BC_652_IR_16_22	0.652	32	≈ 1000	0.16	2.2
BC_652_IR_16_28	0.652	40	≈ 1000	0.16	2.8
BC_702_IR_8_16	0.702	45	≈2000	0.08	1.6
BC_702_IR_8_22	0.702	62	≈2000	0.08	2.2
BC_702_IR_8_28	0.702	78	≈2000	0.08	2.8
BC_702_IR_16_16	0.702	23	≈ 1000	0.16	1.6
BC_702_IR_16_22	0.702	32	≈ 1000	0.16	2.2
BC_702_IR_16_28	0.702	40	≈ 1000	0.16	2.8

Table 3 - Test series A (irregular wave sets) for Raversijde (R) configuration

Wave Set	Water depth at paddle (m)	Duration (min)	Number of Waves	$H_{m0,ss}$ (m)	$T_{p,ss}$ (s)
R_708_IR_8_16	0.708	45	≈2000	0.08	1.6
R_708_IR_8_22	0.708	62	≈2000	0.08	2.2
R_708_IR_8_28	0.708	78	≈2000	0.08	2.8
R_708_IR_12_16	0.708	45	≈2000	0.12	1.6
R_708_IR_12_22	0.708	62	≈2000	0.12	2.2
R_708_IR_12_28	0.708	78	≈2000	0.12	2.8
R_708_IR_16_16	0.708	23	≈ 1000	0.16	1.6
R_708_IR_16_22	0.708	32	≈ 1000	0.16	2.2
R_708_IR_16_28	0.708	40	≈ 1000	0.16	2.8

Table 4 - Test series A (irregular wave sets) for Katwijk (K) configuration

Wave Set	Water depth at paddle (m)	Duration (min)	Number of Waves	$H_{m0,ss}$ (m)	$T_{p,ss}$ (s)
K_708_IR_8_16	0.708	45	≈ 2000	0.08	1.6
K_708_IR_8_22	0.708	62	≈ 2000	0.08	2.2
K_708_IR_8_28	0.708	78	≈ 2000	0.08	2.8
K_708_IR_12_16	0.708	45	≈ 2000	0.12	1.6
K_708_IR_12_22	0.708	62	≈ 2000	0.12	2.2
K_708_IR_12_28	0.708	78	≈ 2000	0.12	2.8
K_708_IR_16_16	0.708	23	≈ 1000	0.16	1.6
K_708_IR_16_22	0.708	32	≈ 1000	0.16	2.2
K_708_IR_16_28	0.708	40	≈ 1000	0.16	2.8
K_738_IR_8_16	0.738	45	≈ 2000	0.08	1.6
K_738_IR_8_22	0.738	62	≈ 2000	0.08	2.2
K_738_IR_8_28	0.738	78	≈ 2000	0.08	2.8
K_738_IR_16_16	0.738	45	≈ 1000	0.16	1.6
K_738_IR_16_22	0.738	62	≈ 1000	0.16	2.2
K_738_IR_16_28	0.738	78	≈ 1000	0.16	2.8

In **test series B** (Table 5 and Table 6), bichromatic wave conditions were considered. The periods of the individual waves forming the bichromatic wave field, T_1 and T_2, were constant for all bichromatic cases, and chosen to form identical wave groups, with an integer number of waves fitting in each group (7 waves per group). For all the bichromatic wave cases, the offshore variance ($m_0 = \frac{H_1^2}{8} + \frac{H_2^2}{8}$, where H_1 and H_2 are the heights of the 2 components forming the bichromatic wave field) was furthermore kept constant. The different bichromatic conditions differ in terms of wave group envelope amplitude (see variations in $\frac{H_2}{H_1}$ between the

cases, with case 0.8 having the largest wave group modulation and 0.4 the smallest). Each condition was furthermore re-run for three values of the phase differences between the primary components ($0^{\circ}, 90^{\circ}, 180^{\circ}$ phase differences), modifying the positions of the waves within the group.

Table 5 - Test series B (bichromatic wave sets) for (reference) base case configuration (BC); H_1 and H_2 are the wave height of the wave components forming the bichromatic signal, T_1 and T_2 the corresponding periods. The phase difference between the two components is also indicated.

Wave Set	Water depth at paddle (m)	Duration (min)	Modulation (H_2/H_1)	H_1 (m)	T_1 (s)	H_2 (m)	T_2 (s)	Phase Difference (°)
BC_652_BCH_WS1_0	0.652	10	0.4	0.18	2.2	0.072	2.64	0
BC_652_BCH_WS1_90	0.652	10	0.4	0.18	2.2	0.072	2.64	90
BC_652_BCH_WS1_180	0.652	10	0.4	0.18	2.2	0.072	2.64	180
BC_652_BCH_WS2_0	0.652	10	0.6	0.18	2.2	0.108	2.64	0
BC_652_BCH_WS2_90	0.652	10	0.6	0.18	2.2	0.108	2.64	90
BC_652_BCH_WS2_180	0.652	10	0.6	0.18	2.2	0.108	2.64	180
BC_652_BCH_WS3_0	0.652	10	0.8	0.18	2.2	0.144	2.64	0
BC_652_BCH_WS3_90	0.652	10	0.8	0.18	2.2	0.144	2.64	90
BC_652_BCH_WS3_180	0.652	10	0.8	0.18	2.2	0.144	2.64	180
BC_702_BCH_WS1_0	0.702	10	0.4	0.18	2.2	0.072	2.64	0
BC_702_BCH_WS1_90	0.702	10	0.4	0.18	2.2	0.072	2.64	90
BC_702_BCH_WS1_180	0.702	10	0.4	0.18	2.2	0.072	2.64	180
BC_702_BCH_WS2_0	0.702	10	0.6	0.18	2.2	0.108	2.64	0
BC_702_BCH_WS2_90	0.702	10	0.6	0.18	2.2	0.108	2.64	90
BC_702_BCH_WS2_180	0.702	10	0.6	0.18	2.2	0.108	2.64	180
BC_702_BCH_WS3_0	0.702	10	0.8	0.18	2.2	0.144	2.64	0
BC_702_BCH_WS3_90	0.702	10	0.8	0.18	2.2	0.144	2.64	90
BC_702_BCH_WS3_180	0.702	10	0.8	0.18	2.2	0.144	2.64	180

Table 6 - Test series B (bichromatic wave sets) for Katwijk configuration

Wave Set	Water depth at paddle (m)	Duration (min)	Modulation (H_2/H_1)	H_1 (m)	T_1 (s)	H_2 (m)	T_2 (s)	Phase Difference (°)
K_708_BCH_WS1_0	0.708	10	0.4	0.18	2.2	0.072	2.64	0
K_708_BCH_WS1_90	0.708	10	0.4	0.18	2.2	0.072	2.64	90
K_708_BCH_WS1_180	0.708	10	0.4	0.18	2.2	0.072	2.64	180
K_708_BCH_WS2_0	0.708	10	0.6	0.18	2.2	0.108	2.64	0
K_708_BCH_WS2_90	0.708	10	0.6	0.18	2.2	0.108	2.64	90
K_708_BCH_WS2_180	0.708	10	0.6	0.18	2.2	0.108	2.64	180
K_708_BCH_WS3_0	0.708	10	0.8	0.18	2.2	0.144	2.64	0
K_708_BCH_WS3_90	0.708	10	0.8	0.18	2.2	0.144	2.64	90
K_708_BCH_WS3_180	0.708	10	0.8	0.18	2.2	0.144	2.64	180

In **test series C** (Table 7, Table 8, and Table 9), a bimodal spectrum was imposed at the wave paddle to schematize a situation combining a sea-swell wave peak and a free (remotely-generated) infragravity wave peak. The sea-swell wave peak was schematized as in Series A using a JONSWAP spectrum with a peak enhancement factor of 3.3. For the free infragravity wave peak, a Gaussian spectrum was imposed with peak frequencies defined as 8.8 and 13.2 s. In Figure 12, a sketch showing the bimodal shape of the target spectrum for the Katwijk configuration for wave set K_708_IG2_16_22 is presented as an example. It considers 16 cm significant wave height ($H_{m0,ss}$) and 2.2 s peak wave period ($T_{p,ss}$) in the high frequency band for the sea-swell waves and 3 cm significant wave height ($H_{s,FIG}$) and 13.2 s peak wave period ($T_{p,FIG}$) for the free IG waves.

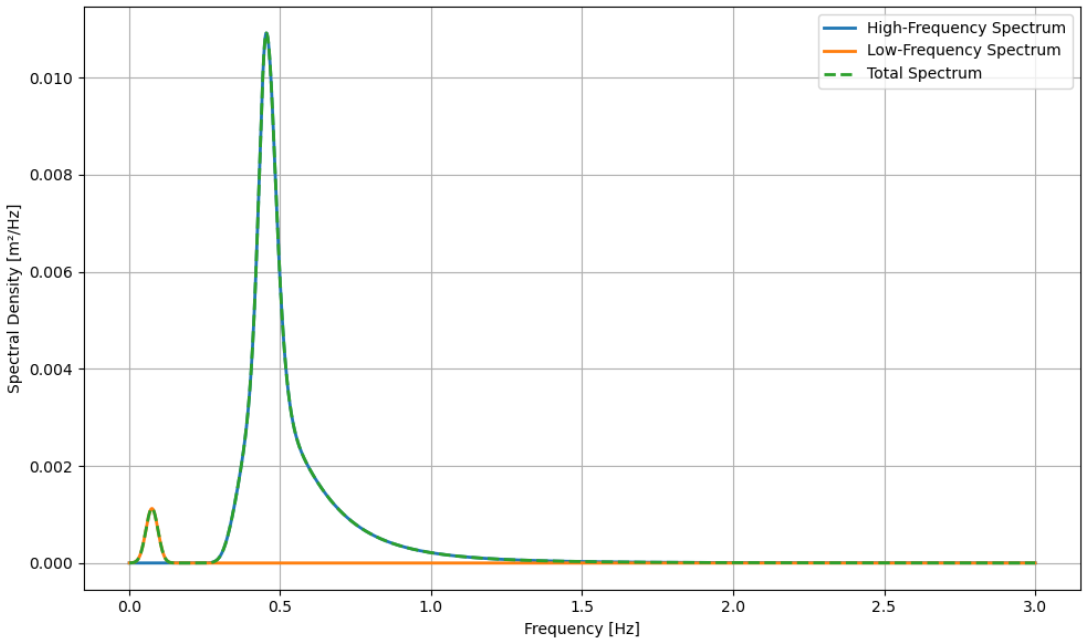

Figure 12 – Target spectrum for the bimodal spectrum wave set for Katwijk configuration for K_708_IG2_16_22 wave set case

Table 7 - Test series C (bimodal spectrum wave sets, including free IG waves) for the base case (BC) configuration

Wave Set	Water depth at paddle (m)	Duration (min)	Number of Waves	$H_{m0,SS}$ (m)	$T_{p,SS}$ (s)	$H_{m0,FIG}$ (m)	$T_{p,FIG}$ (s)
BC_652_IG1_8_22	0.652	62	≈ 2000	0.08	2.2	0.03	8.8
BC_652_IG1_10_22	0.652	32	≈ 1000	0.10	2.2	0.03	8.8
BC_702_IG1_8_22	0.702	62	≈ 2000	0.08	2.2	0.03	8.8
BC_702_IG2_8_22	0.702	62	≈ 2000	0.08	2.2	0.03	13.6
BC_702_IG1_10_22	0.702	32	≈ 1000	0.10	2.2	0.03	8.8
BC_702_IG2_10_22	0.702	32	≈ 1000	0.10	2.2	0.03	13.6

Table 8 - Test series C (bimodal spectrum wave sets, including offshore free IG waves) for the Raversijde (R) configuration

Wave Set	Water depth at paddle (m)	Duration (min)	Number of Waves	$H_{m0,SS}$ (m)	$T_{p,SS}$ (s)	$H_{m0,FIG}$ (m)	$T_{p,FIG}$ (s)
R_708_IG1_8_22	0.708	62	≈ 2000	0.08	2.2	0.03	8.8
R_708_IG2_8_22	0.708	62	≈ 2000	0.08	2.2	0.03	13.2
R_708_IG1_16_22	0.708	32	≈ 1000	0.16	2.2	0.03	8.8
R_708_IG2_16_22	0.708	32	≈ 1000	0.16	2.2	0.03	13.2

Table 9 - Test series C (bimodal spectrum wave sets, including offshore free IG waves) for the Katwijk (K) configuration

Wave Set	Water depth at paddle (m)	Duration (min)	Number of Waves	$H_{m0,SS}$ (m)	$T_{p,SS}$ (s)	$H_{m0,FIG}$ (m)	$T_{p,FIG}$ (s)
K_708_IG1_8_22	0.708	62	≈ 2000	0.08	2.2	0.03	8.8
K_708_IG2_8_22	0.708	62	≈ 2000	0.08	2.2	0.03	13.2
K_708_IG1_16_22	0.708	32	≈ 1000	0.10	2.2	0.03	8.8
K_708_IG2_16_22	0.708	32	≈ 1000	0.10	2.2	0.03	13.2
K_738_IG1_8_22	0.738	62	≈ 2000	0.08	2.2	0.03	8.8
K_738_IG2_8_22	0.738	62	≈ 2000	0.08	2.2	0.03	13.2
K_738_IG1_16_22	0.738	32	≈ 1000	0.10	2.2	0.03	8.8
K_738_IG2_16_22	0.738	32	≈ 1000	0.10	2.2	0.03	13.2

5. Data post-processing and first visualizations

All instruments (except for the LED-PIV system) return values in voltages that need to be calibrated before use. The calibration procedures and resulting calibration curves are presented in Annex B – Calibration coefficients for laboratory instruments. For the large majority of the instruments (all instruments except for 3 pressure sensors that may require recalibration), the calibration procedure resulted in a well-fitting linear calibration curves.

Some first data visualizations for the wave set R_708_IG2_16_22 are presented below to demonstrate data quality and illustrate the range of measurements carried out during the physical modeling campaign.

Figure 13 shows examples of collocated velocity (red) and elevation (blue) timeseries at two locations along the flume, one on the offshore horizontal part (top panel), and one at the start of the surf zone (lower panel). As expected these timeseries are roughly in phase, and the waves become increasingly asymmetric when they approach the shore.

As a consistency check, the cross-shore evolution of the significant wave height, calculated from the total surface elevation timeseries, is presented in Figure 14. The offshore wave height is very close to the target significant wave height of 16 cm for this wave set. The significant wave height starts decaying around x=20m, consistent with the observation during the experiments that waves started breaking near the offshore edge of the foreshore. The local increase in wave height at the toe of the dike (WG14, x≈32m) is likely due to reflection patterns, as this increase was not observed when this wave set was repeated without the dike in Phase 2 of the experiments (not shown).

The two types of pressure sensors deployed on the dike to measure impacts are compared in Figure 15. Here we show as an example the lower sensors of each pressure sensor line (Kulite 1 and Honeywell 1), located in a still water depth of about 4cm for this specific wave set. It should be noted that, besides applying the calibration curve presented in Annex B, an additional offset correction was applied to ensure that the initial pressure head measured at the sensor matched the known still water level. After correcting for the initial pressure difference, both signal exhibit oscillations with very similar magnitude and shape. The maximum pressure head value reached for each individual wave is consistently predicted by both sensor types, while some discrepancies appear in the wave troughs.

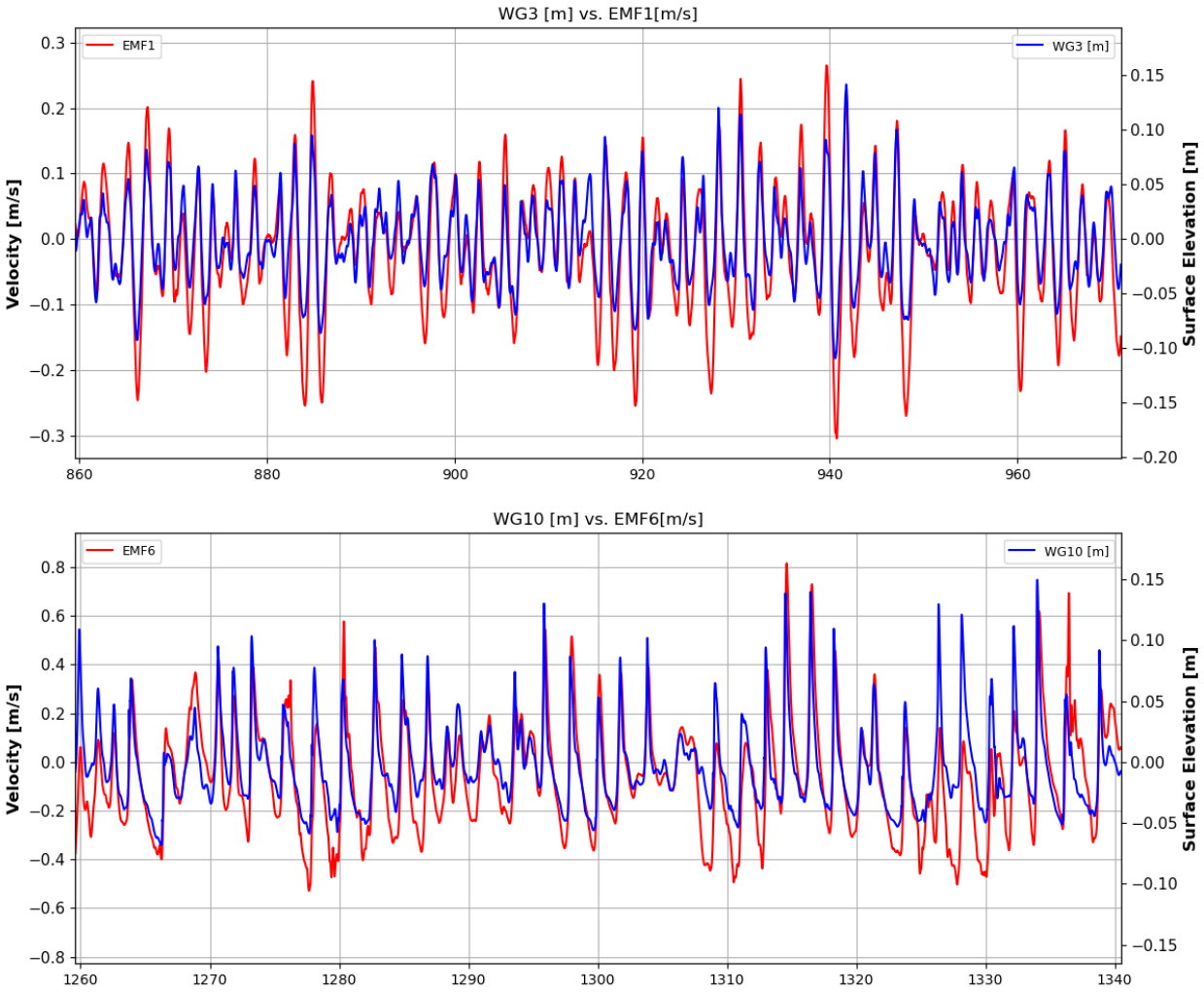

Figure 13 - Calibrated results from WG3 and EMF1, located 7.14 m from the wave flume's reference point (x = 0 m) (Top panel), and calibrated results from WG10 and EMF6, located 24.7 m from the wave flume's reference point (x = 0 m) (Bottom panel)

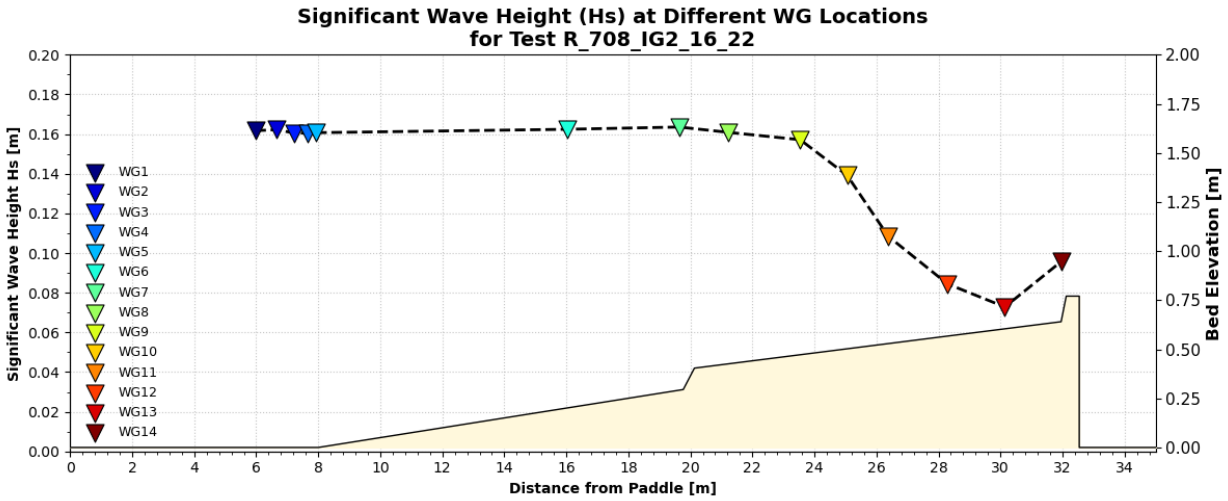

Figure 14 – Evolution of significant wave height (H_s) along the flume for test case R_708_IG2_16_22, with offshore boundary conditions of $H_s = 0.16\ m$ and $T_p = 2.2\ s$. The Hs values in the plot is calculated by integrating over the entire frequency band resolved by the Welch spectrum. The total spectral energy $E_{total} = \int S(f)\, df$ is used to compute $H_s = \sqrt{16E_{total}}$, without restricting the integration to a specific frequency band (e.g., IG or sea–swell only)

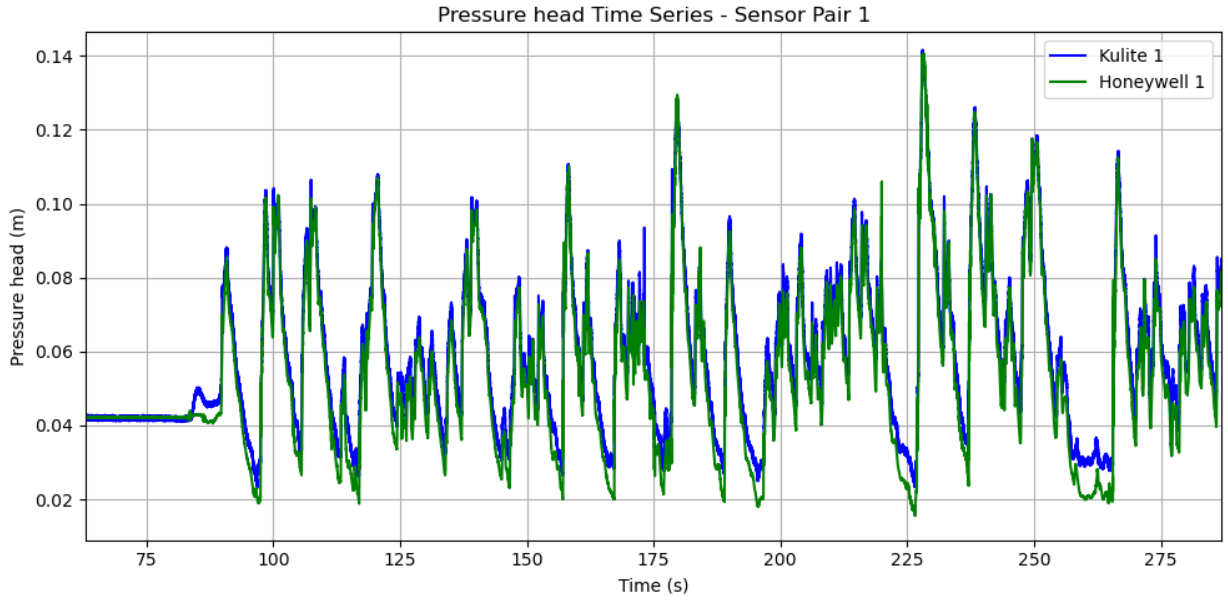

Figure 15 – Calibrated results of the Honeywell 1 and Kulite 1 pressure sensors. The figure shows the pressure head, defined as p(t)/ρg, with ρ the water density and g the gravitational acceleration. The signal is corrected using a constant offset to ensure that the initial pressure sensor head corresponds to the still water level at the top of the sensor at the start of the test (0.042 m).

Finally, Figure 16 presents measurements performed in the overtopping tank during the same wave set. It shows how the water level in the tank increases in time as a result of successive overtopping events. Two instruments are compared here, a wave gauge (WG 15) and an ultrasonic sensor (MIC 3). The raw data from the ultrasonic sensor was significantly more noisy than the wave gauge data (see purple dashed line). However, after proper filtering, both instruments exhibit very similar patterns (solid lines), giving confidence on the usability of the 3 ultrasonic sensors in future analyses.

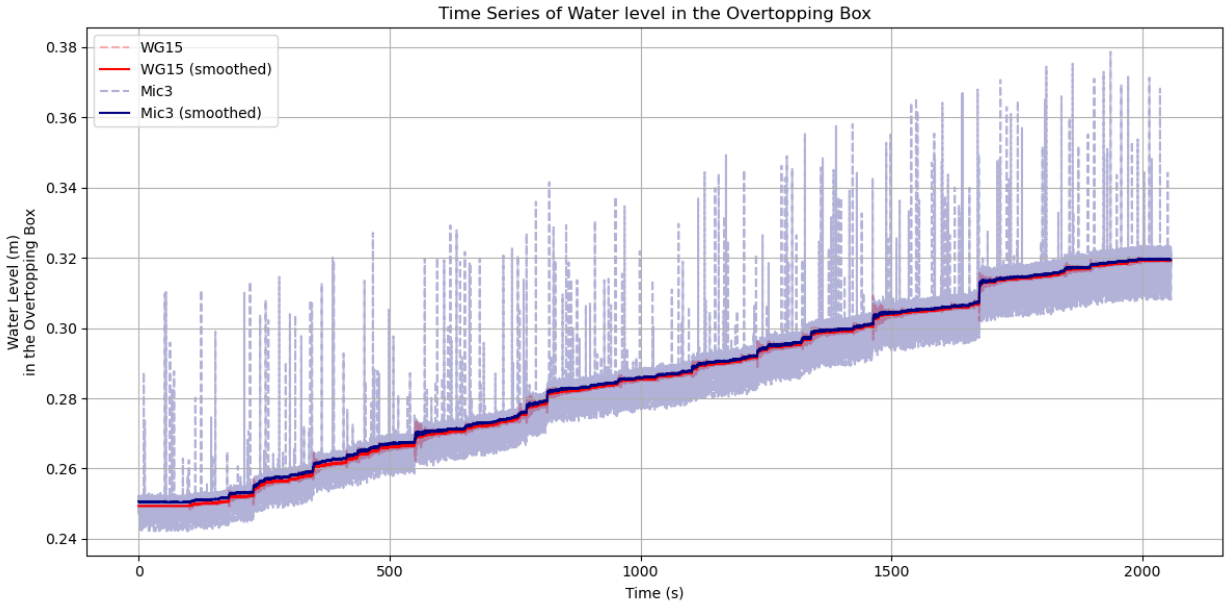

Figure 16 – Calibrated overtopping measurements for test R_708_IG2_16_22. ***The red line*** *represents the smoothed results from WG 15, and* ***the blue line*** *shows the smoothed results from MIC 3. Water level time series smoothed using a Savitzky–Golay filter (window = 1001 samples, polynomial order = 5) to preserve peak structure while suppressing noise.*

6. Dataset structure and archiving

During the physical modeling campaign, a total of 168 tests were carried out. Eighty-four of those were carried out in Phase 1 (with the dike), and 84 were carried out in Phase 2 (after removing the dike). All gathered data are organised into a single parent directory. Within this directory, each test have its own folder, containing the measured data. The naming convention for the tests folders is described in Section 6.1, while the content of these individual folders is described in Section 6.2, including an overview of different data files and a description of their structure.

6.1 Naming of the data folders

For **Test Series A** (irregular wave sets), an example is given below to explain the naming format;

T_001_BC_652_IR_8_16

In this naming,

- T stands for "Test".
- A 3-digit number (for instance, 001, 084, 122, and so on) shows the number of the order in which the tests were conducted. Test numbers increase sequentially based on the order in which the tests were conducted.
- BC represents the Base (Reference) Case slope; R and K were used for the Raversijde and Katwijk slopes, respectively.
- 652 (also 702, 708, and 738) represents the still water depth in mm at the offshore part of the flume.
- IR indicates that the test series is an irregular wave set.
- IR_8_16 represents that the test series is an irregular wave set with significant wave height (H_s) as 8 cm and spectral peak wave period (T_p) as 1.6 s.

For **Test Series B** (bichromatic wave sets), an example is given below to explain the naming format;

T_052_R_652_BCH_WS_3_90

In this naming,

- T stands for "Test".
- A 3-digit number (for instance, 001, 052, 122, and so on) shows the number of the order in which the tests are conducted. Test numbers increase sequentially based on the date and order in which the tests are conducted.
- R represents the Raversijde slope.

- BCH indicates that the test series is a bichromatic wave set.
- WS_3_90 indicates the modulation (ratio) of individual wave heights, and the phase difference (in °) between these waves. WS_1, WS_2, and WS_3 represent 0.4, 0.6, and 0.8 modulation (ratio), respectively. Three different phase differences, which are 0°, 90° and 180° were considered. The phase difference that was applied in the wave set is indicated by the last term of the name of the file.

For **Test Series C** (bimodal wave sets, including free IG waves), an example is given below to explain the naming format;

In this naming,

T_068_K_708_IG1_8_22

- T stands for "Test".
- A 3-digit number (for instance, 001, 084, 122, and so on) shows the number of the order in which the tests are conducted. Test numbers increase sequentially based on the date and order in which the tests are conducted.
- K represents the Katwijk slope
- 652 (also 702, 708, and 738) represents the considered water depth in mm at the offshore part of the flume.
- IG1 indicates that the test series is a bimodal wave set with a free IG significant wave height ($H_{m0,FIG}$) of 3 cm and a spectral peak wave period ($T_{p,FIG}$) of 8.8 s. For IG2, the free IG significant wave height ($H_{m0,FIG}$) is 3 cm and and spectral peak wave period ($T_{p,FIG}$) is 13.2 s.
- IG1_8_22 indicates that the target sea-swell significant wave height ($H_{m0,SS}$) is 8 cm and the spectral peak wave period ($T_{p,SS}$) is 2.2 s.

For Phase 2 tests, "ND" (No Dike) is added at the end of the folder names to indicate that this wave set belongs to Phase 2, in which the dike model is not included.

6.2 Content of the data folders

Three ASCII files can be found in each data folder, containing the timeseries (in Volts) recorded by:

- the pressure sensors (file name "**Pressure"**)
- the wave gauges (file name **WG**)
- the electromagnetic flowmeters (EMF) and ultrasonic sensors (MIC) (combined in one file called "**EMF_Mic**").

The **"Pressure"** and **"WG"** files consists of 17 columns, while the **"EMF_MIC"** file includes 15 columns of data.

For the **"Pressure"** files:

- The first column is the time in seconds
- The second to ninth columns are the voltage values from the Kulite pressure sensors (Kulite 1-8). The pressure sensors are ordered from bottom to top (sensor at the bottom, Kulite 1, and sensor at the top, Kulite 8)
- The tenth to seventeenth (the last column) columns are the voltage values from the Honeywell pressure sensors (Honeywell 1-8). The pressure sensors are ordered from bottom to top (sensor at the bottom, Honeywell 1, and sensor at the top, Honeywell 8)

For the **"WG"** files:

- The first column is the time in seconds
- The second to sixteenth columns are the voltage values from the wave gauges (WG 1-15) along the wave flume, starting from the first one located nearest to the generator at offshore (WG 1) to wave gauge inside the wave overtopping box (WG 15).
- The last column of the file is the data measured by the wave gauge located on the wave paddle.

For **"EMF_Mic"** files:

- The first column is the time in seconds
- The second to tenth columns are the voltage values from the electromagnetic flow meters (EMF 1-9) along the wave flume, starting from the first one located nearest to the generator at offshore (EMF 1) to the nearest to the dike model (EMF 9).
- The eleventh to thirteenth columns are the voltage values from ultrasonic sensors (MIC 1-3), starting from the closest ultrasonic sensor to the seaward side of the crest to the inside of the overtopping box.
- The fourteenth and fifteenth columns are the voltage values from the reference Kulite pressure sensors located in water and air, respectively, at the back side of the model section.

6.3 Calibration files

In addition to these, 11 different calibration files are provided. Six of these files are for the wave gauges. For every slope configuration during both Phase 1 and Phase 2, calibration measurements were taken for the wave gauges (see Annex B for more information). These six files are listed below:

- **Base_Case_End** (Base Case slope for Phase 1)
- **Raversijde_Start**(Raversijde slope for Phase 1)
- **Katwijk_Start** (Katwijk slope for Phase 1)
- **Base_Case_No_Dike** (Base Case slope for Phase 2)
- **Raversijde_No_Dike** (Raversijde slope for Phase 2)
- **Katwijk_No_Dike** (Katwijk slope for Phase 2)

All pressure sensors were calibrated at the same time once. For all wave sets in Phase 1, the calibration file **"Main_Pressure_Sensors"** is available.

The 2 ultrasonic sensors on the crest of the dike model and the ultrasonic sensor above the overtopping box were calibrated once and separately. For all wave sets in Phase 1, the calibration file **"Second_Mics_Calibration"** and **"Second_Overtopping_Tank_Calibration"** files can be used for the ultrasonic sensors on the crest and the ultrasonic sensor inside the overtopping box, respectively.

In Table 10 and

Table 11, the test number ranges with the corresponding calibration dataset and the meanings of the abbreviations and numeric codes are presented.

Table 10 – Test number ranges with the corresponding calibration dataset

Test Number Range	**Suitable Calibration Dataset for WGs**	**Suitable Calibration Dataset for Ultrasonics**	**Suitable Calibration Dataset for Pressure Sensors**
From T_001 to T_039	Base_Case_End / Second_Overtopping_Tank_Calibration	Second_Mics_Calibration / Second_Overtopping_Tank_Calibration	Main_Pressure_Sensors / Pressure_diff_compensators
From T_040 to T_052	Raversijde_Start / Second_Overtopping_Tank_Calibration	Second_Mics_Calibration / Second_Overtopping_Tank_Calibration	Main_Pressure_Sensors / Pressure_diff_compensators
From T_053 to T_084	Katwijk_Start / Second_Overtopping_Tank_Calibration	Second_Mics_Calibration / Second_Overtopping_Tank_Calibration	Main_Pressure_Sensors / Pressure_diff_compensators
From T_084 to T_116	Katwijk_No_Dike	Microsonic_No_Dike	-
From T_117 to T_129	Raversijde_No_Dike	Microsonic_No_Dike	-
From T_130 to T_168	Base_Case_No_Dike	Microsonic_No_Dike	-

Table 11 – Meaning of abbreviations or numeric codes in the folder names

Abbreviation in Folder Name	Description
T	Test
BC	Base Case
R	Raversijde
K	Katwijk
ND	No dike (for Phase 2 tests)
IR	Irregular wave set
BCH	Bichromatic wave set
WS	Wave set
WS3_180	Bichromatic wave set with 0.8 modulation and 180° phase difference
IG	Bimodal wave set
IR_8_22	Irregular waves ($T_{p,ss}$ = 2.2 s, $H_{m0,ss}$ = 0.08 m)
IG1_8_22	Bimodal save set
WG	Wave gauge
MIC	Ultrasonic sensor

7. Data Availability

All the gathered datasets, except LED-PIV measurements, were uploaded to 4TU.ResearchData, as raw data, along with a copy of the present report. The dataset for this deliverable can be found from the following link: https://doi.org/10.4121/28d01946-3094-4dcb-8548-02085338d3ef.

All gathered data are organised into a single parent directory. Within this directory, each test has its own folder, containing the measured data in ASCII format for pressure, water surface elevation, and flow velocity measurements given in voltage values. It is recommended to read the README.md file and the present report before using the dataset. The dataset will be under embargo until June 2028, until the end of the DuneFront project.

References

Akrish, G., A. Reniers, D. Rijnsdorp, M. Zijlema, J. Rutten, & M. Tissier (under review). The importance of free infragravity waves in the North Sea: Insights from field observations and unstructured SWAN modelling.

Bakker, W, B Hofland, E de Almeida, G Oldenziel and E F J Overmars (2025) Pulsed LED line light for large-scale PIV—development and use in wave load measurements. Meas. Sci. Technol. 32 (2021) 115205 (12pp). https://doi.org/10.1088/1361-6501/ac17ce

Buckley, M. L., R. J. Lowe, J. E. Hansen, & A. Van Dongeren (2015). Dynamics of Wave Setup over a Steeply Sloping Fringing Reef. *J. Phys. Oceanogr.*, **45**, 3005–3023.

Eldrup, M. R., & Andersen, T. L. (2019). Extension of shallow water rock armour stability formulae to nonlinear waves. *Coastal Engineering*, *153*, 103536.

Guza, R. T., Thornton, E. B., & Holman, R. A. (1985). Swash on steep and shallow beaches. In *Coastal Engineering 1984* (pp. 708-723).

Reniers, A. J., R. Naporowski, M. Tissier, M. de Schipper, G. Akrish & D.P. Rijnsdorp (2021). North Sea infragravity wave observations. *Journal of Marine Science and Engineering*, *9*(2), 141.

Rijnsdorp, D. P., A. Reniers & M. Zijlema (2021). Free infragravity waves in the North Sea. *Journal of Geophysical Research: Oceans*, *126*(8), e2021JC017368.

Roelvink, D, A. Reniers, A. van Dongeren, J. van Thiel de Vries, R. McCall & J. Lescinski (2009) Modelling storm impacts on beaches, dunes and barrier islands Coast. Eng. **56** 1133–52.

Sevindik, C., B. Hofland, M. Tissier, A. Adeli, P. Troch, V. Gruwez & O. Lojek. (2024) Boundary conditions under extreme storms for the physical modelling of dike-dune Demonstrators. DuneFront report D7.2, Version 1.0.

Annex A – Positions of the wave gauges and electromagnetic flow meters

In the following, the x-position is defined with respect to a reference point located two meters in front of the zero-position of the wave generator (in this reference frame, the generator is therefore at x=-2m).

Table 12 – Positions of the WGs to the reference point (x = 0 m) for both Phase 1 and Phase 2

Base (Reference) Case Profiles		Raversijde and Katwijk Profiles	
Wave Gauge	**Distance (m)**	**Wave Gauge**	**Distance (m)**
WG-1	5.97	WG-1	5.97
WG-2	6.67	WG-2	6.67
WG-3	7.21	WG-3	7.21
WG-4	7.63	WG-4	7.63
WG-5	7.95	WG-5	7.95
WG-6	16.05	WG-6	16.05
WG-7	19.63	WG-7	19.63
WG-8	21.35	WG-8	21.35
WG-9	23.68	WG-9	23.68
WG-10	25.19	WG-10	25.19
WG-11	26.52	WG-11	26.52
WG-12	28.40	WG-12	28.40
WG-13	30.25	WG-13	30.25
WG-14	31.98	WG-14	32.15
WG-15*	33.66	WG-15	33.66

*) WG-15 was removed after removing the dike section and the overtopping box and not used in Phase 2

Table 13 - – Positions of the EMFs to the reference point (x = 0 m) for all bed profiles, for Phase 1 and Phase 2

Electromagnetic Flow Meter	Distance (m)
EMF-1	7.21
EMF-2	16.05
EMF-3	19.63
EMF-4	21.35
EMF-5	23.68
EMF-6	25.19
EMF-7	26.52
EMF-8	28.40
EMF-9	30.25

Table 14 – Distances of EMF measurement points to the bottom for Phase 1

Base (Reference) Case Profile		Raversijde Slope		Katwijk Slope	
EMF	Distance (cm)	EMF	Distance (cm)	EMF	Distance (cm)
EMF-1	35	EMF-1	35	EMF-1	35
EMF-2	19	EMF-2	19	EMF-2	19
EMF-3	19	EMF-3	19	EMF-3	20
EMF-4	6	EMF-4	6	EMF-4	6
EMF-5	6	EMF-5	6	EMF-5	6
EMF-6	6	EMF-6	6	EMF-6	6
EMF-7	6	EMF-7	6	EMF-7	6
EMF-8	6	EMF-8	6	EMF-8	3
EMF-9	6	EMF-9	6	EMF-9	3

Table 15 – Distances of EMF measurement points to the bottom for Phase 2

Base (Reference) Case Profile		Raversijde Slope		Katwijk Slope	
EMF	Distance (cm)	EMF	Distance (cm)	EMF	Distance (cm)
EMF-1	35	EMF-1	35	EMF-1	35
EMF-2	19	EMF-2	19	EMF-2	19
EMF-3	20	EMF-3	20	EMF-3	20
EMF-4	6	EMF-4	6	EMF-4	6
EMF-5	6	EMF-5	6	EMF-5	6
EMF-6	6	EMF-6	6	EMF-6	6
EMF-7	6	EMF-7	7	EMF-7	7
EMF-8	6	EMF-8	3.5	EMF-8	3.5
EMF-9	6	EMF-9	3.5	EMF-9	3.5

Annex B – Calibration coefficients for laboratory instruments

B1. Wave Gauges

In our physical modelling experiments, accurate wave gauge calibration is essential for reliable measurement of water surface elevation. To achieve this, we performed a series of controlled calibration procedures in the wave flume. The calibration process involved gradually reducing the still water level in the flume in a stepwise manner. At each fixed water level, voltage readings from the wave gauges were recorded under still-water conditions. This allowed us to establish a direct relationship between the known water depth and the raw voltage output of the gauges.

A total of seven distinct calibration datasets were collected throughout the experimental campaign (reported in The only exception here is the “Base_Case_Start” file. This measurement was taken before starting the experiments, and after that, some of the wave gauges were lowered. Due to this situation, a new calibration measurement (Base_Case_End) was taken.

Table 16). A new calibration set was acquired after any significant alteration to the bathymetry of the physical model, as part of the sensors had to be repositioned following bottom alterations. During the changing of the bathymetries and phases, wave gauges were located at the same locations and at almost the same depths. So, the calibration formula derived from a specific dataset can be applied to the same bathymetric configurations from Phases 1 and 2. For instance, “Base_Case_End” and “Base_Case_No_Dike” can be applied to the test results of the Base Case bathymetric configuration from both Phases 1 and 2. The only exception here is the “Base_Case_Start” file. This measurement was taken before starting the experiments, and after that, some of the wave gauges were lowered. Due to this situation, a new calibration measurement (Base_Case_End) was taken.

Table 16 – List of calibration tests

Num.	Date of Conduct	Test name	Description
1	08/April/2025	Base_Case_Start	Calibration test at the beginning of the base case modelling
2	16/April/2025	Base_Case_End	Calibration test at the End of the base case modelling
3	16/April/2025	Raversijde_Start	Calibration test at the beginning of the Raversijde modelling
4	23/April/2025	Katwijk_Start	Calibration test at the beginning of the Katwijk modelling
5	14/May/2025	Katwijk_No_Dike	Calibration test after removing the dike and at the beginning of the Katwijk modelling
6	16/May/2025	Raversijde_No_Dike	Calibration test after removing the dike and at the beginning of the Raversijde modelling
7	21/May/2025	Base_Case_No_Dike	Calibration test after removing the dike and at the beginning of the Base case modelling

Calibration Methodology Using a Linear Model

To establish a quantitative relationship between the mean voltage readings of each wave gauge and the corresponding water level during calibration, a linear regression approach was adopted.

For each gauge, the mean voltage recorded at various known water levels forms the dataset. Denoting the mean voltage for the *i*-th calibration step as V_i and the corresponding water level as h_i, the calibration data for each gauge is modeled as:

$$h_i = a + bV_i$$

where:

- h_i : true water level (m)
- V_i : measured mean voltage (V)
- a: intercept (offset) (m)
- b: slope (calibration coefficient, m/V)

A **linear regression** is performed using the least-squares method to determine the optimal values of **a** and **b**. This fitted linear model enables direct conversion of raw voltage readings into water levels during experimental runs by applying the derived calibration equation (Table 17).

This method is robust, easy to interpret, and widely accepted for calibrating wave gauges where the response is predominantly linear within the calibration interval. The fit quality can be visually inspected by comparing the predicted and measured water levels (see example in Figure 17).

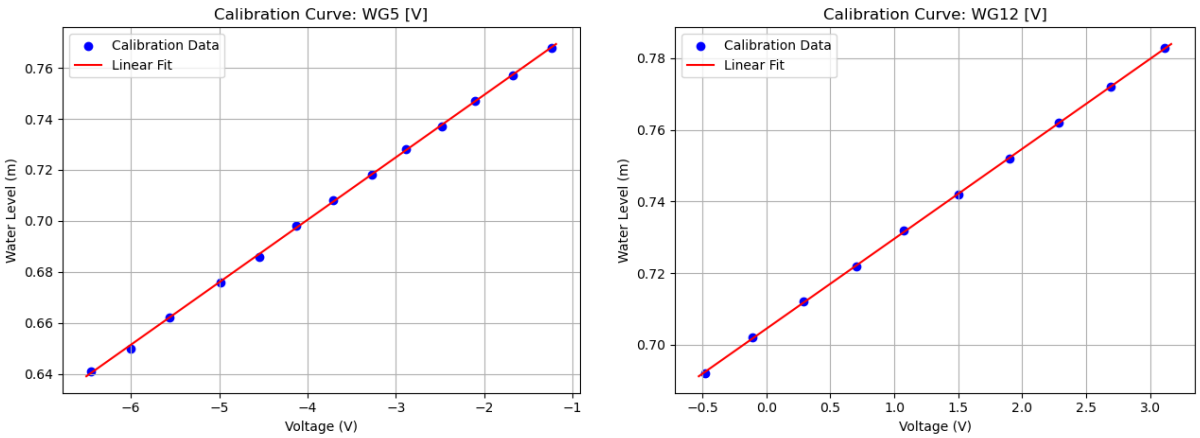

*Figure 17 - **Left Panel**: calibration plot of wave gauge 5 for calibration test at the beginning of the base case modelling, **Right Panel**: calibration plot of wave gauge 12 for calibration test after removing the dike and at the beginning of the Raversijde modelling*

Table 17 - Calibration formulas for the wave gauges

Num.	Test name	Calibration Formula
1	Base_Case_Start	WG1_level(m) = 0.7437 + 0.0245 × voltage(V) WG2_level(m) = 0.7715 + 0.0247 × voltage(V) WG3_level(m) = 0.7410 + 0.0253 × voltage(V) WG4_level(m) = 0.7668 + 0.0246 × voltage(V) WG5_level(m) = 0.7984 + 0.0245 × voltage(V) WG6_level(m) = 0.7765 + 0.0246 × voltage(V) WG7_level(m) = 0.7976 + 0.0245 × voltage(V) WG8_level(m) = 0.7885 + 0.0249 × voltage(V) WG9_level(m) = 0.7760 + 0.0243 × voltage(V) WG10_level(m) = 0.7805 + 0.0232 × voltage(V) WG11_level(m) = 0.6312 + 0.0247 × voltage(V) WG12_level(m) = 0.6040 + 0.0247 × voltage(V) WG13_level(m) = 0.6457 + 0.0245 × voltage(V) WG14_level(m) = 0.6521 + 0.0252 × voltage(V)
2	Base_Case_End	WG1_level(m) = 0.7442 + 0.0247 × voltage(V) WG2_level(m) = 0.7701 + 0.0246 × voltage(V) WG3_level(m) = 0.7390 + 0.0253 × voltage(V) WG4_level(m) = 0.7676 + 0.0248 × voltage(V) WG5_level(m) = 0.7461 + 0.0246 × voltage(V)

Num.	Test name	Calibration Formula
		WG6_level(m) = 0.7727 + 0.0241 × voltage(V) WG7_level(m) = 0.7487 + 0.0245 × voltage(V) WG8_level(m) = 0.7872 + 0.0248 × voltage(V) WG9_level(m) = 0.7767 + 0.0244 × voltage(V) WG10_level(m) = 0.7819 + 0.0235 × voltage(V) WG11_level(m) = 0.6299 + 0.0250 × voltage(V) WG12_level(m) = 0.6027 + 0.0252 × voltage(V) WG13_level(m) = 0.6461 + 0.0251 × voltage(V) WG14_level(m) = 0.6508 + 0.0264 × voltage(V)
3	Raversijde_Start	WG1_level(m) = 0.7456 + 0.0252 × voltage(V) WG2_level(m) = 0.7731 + 0.0252 × voltage(V) WG3_level(m) = 0.7415 + 0.0259 × voltage(V) WG4_level(m) = 0.7698 + 0.0253 × voltage(V) WG5_level(m) = 0.7481 + 0.0253 × voltage(V) WG6_level(m) = 0.7761 + 0.0248 × voltage(V) WG7_level(m) = 0.7509 + 0.0252 × voltage(V) WG8_level(m) = 0.7907 + 0.0255 × voltage(V) WG9_level(m) = 0.7840 + 0.0248 × voltage(V) WG10_level(m) = 0.8700 + 0.0239 × voltage(V) WG11_level(m) = 0.7120 + 0.0251 × voltage(V) WG12_level(m) = 0.7033 + 0.0253 × voltage(V) WG13_level(m) = 0.7059 + 0.0251 × voltage(V) WG14_level(m) = 0.7142 + 0.0255 × voltage(V)
4	Katwijk_Start	WG1_level(m) = 0.7457 + 0.0250 × voltage(V) WG2_level(m) = 0.7716 + 0.0247 × voltage(V) WG3_level(m) = 0.7423 + 0.0258 × voltage(V) WG4_level(m) = 0.7704 + 0.0251 × voltage(V) WG5_level(m) = 0.7495 + 0.0252 × voltage(V) WG6_level(m) = 0.7748 + 0.0246 × voltage(V) WG7_level(m) = 0.7506 + 0.0251 × voltage(V) WG8_level(m) = 0.8430 + 0.0254 × voltage(V) WG9_level(m) = 0.8660 + 0.0246 × voltage(V) WG10_level(m) = 0.8701 + 0.0238 × voltage(V) WG11_level(m) = 0.7125 + 0.0250 × voltage(V) WG12_level(m) = 0.7040 + 0.0253 × voltage(V) WG13_level(m) = 0.7063 + 0.0250 × voltage(V) WG14_level(m) = 0.7152 + 0.0258 × voltage(V)
5	Katwijk_No_Dike	WG1_level(m) = 0.7457 + 0.0249 × voltage(V) WG2_level(m) = 0.7726 + 0.0249 × voltage(V) WG3_level(m) = 0.7415 + 0.0257 × voltage(V) WG4_level(m) = 0.7700 + 0.0250 × voltage(V) WG5_level(m) = 0.7513 + 0.0252 × voltage(V)

Num.	Test name	Calibration Formula
		WG6_level(m) = 0.7750 + 0.0245 × voltage(V) WG7_level(m) = 0.7500 + 0.0246 × voltage(V) WG8_level(m) = 0.8400 + 0.0249 × voltage(V) WG9_level(m) = 0.8631 + 0.0242 × voltage(V) WG10_level(m) = 0.8695 + 0.0237 × voltage(V) WG11_level(m) = 0.7121 + 0.0248 × voltage(V) WG12_level(m) = 0.7050 + 0.0250 × voltage(V) WG13_level(m) = 0.7060 + 0.0249 × voltage(V) WG14_level(m) = 0.7138 + 0.0249 × voltage(V)
6	Raversijde_No_Dike	WG1_level(m) = 0.7464 + 0.0251 × voltage(V) WG2_level(m) = 0.7727 + 0.0249 × voltage(V) WG3_level(m) = 0.7415 + 0.0257 × voltage(V) WG4_level(m) = 0.7705 + 0.0250 × voltage(V) WG5_level(m) = 0.7527 + 0.0252 × voltage(V) WG6_level(m) = 0.7761 + 0.0247 × voltage(V) WG7_level(m) = 0.7508 + 0.0248 × voltage(V) WG8_level(m) = 0.7888 + 0.0253 × voltage(V) WG9_level(m) = 0.7884 + 0.0247 × voltage(V) WG10_level(m) = 0.8697 + 0.0238 × voltage(V) WG11_level(m) = 0.7117 + 0.0249 × voltage(V) WG12_level(m) = 0.7045 + 0.0251 × voltage(V) WG13_level(m) = 0.7054 + 0.0250 × voltage(V) WG14_level(m) = 0.7133 + 0.0249 × voltage(V)
7	Base_Case_No_Dike	WG1_level(m) = 0.7465 + 0.0251 × voltage(V) WG2_level(m) = 0.7728 + 0.0250 × voltage(V) WG3_level(m) = 0.7418 + 0.0258 × voltage(V) WG4_level(m) = 0.7711 + 0.0253 × voltage(V) WG5_level(m) = 0.7528 + 0.0253 × voltage(V) WG6_level(m) = 0.7761 + 0.0247 × voltage(V) WG7_level(m) = 0.7510 + 0.0250 × voltage(V) WG8_level(m) = 0.7889 + 0.0253 × voltage(V) WG9_level(m) = 0.7867 + 0.0247 × voltage(V) WG10_level(m) = 0.7909 + 0.0236 × voltage(V) WG11_level(m) = 0.6375 + 0.0250 × voltage(V) WG12_level(m) = 0.6087 + 0.0251 × voltage(V) WG13_level(m) = 0.6501 + 0.0252 × voltage(V) WG14_level(m) = 0.6510 + 0.0257 × voltage(V)

B2. Electromagnetic Flow Meters (EMF)

In our physical modeling campaign, we employed Electromagnetic Flow Meters (EMF) to measure the horizontal components of flow velocity in X direction. These sensors operate in

either voltage mode or velocity mode. In our experiments, the EMF units were used in **voltage mode**, meaning the output is measured in volts and must be converted to velocity (m/s) using calibration functions.

Each EMF device was calibrated by Deltares in a controlled flume environment, with known reference velocities (V) applied and corresponding voltage outputs (U) recorded. A sample EMS calibration certificate (for unit E661, see Figure 18) shows that the conversion from voltage to velocity follows a **second-order polynomial function** of the form:

- **X-direction**: $|V|=-0.000188\ U^2+0.1023\ |U|+0.002$ [m/s]
- **Y-direction**: $|V|=-0.001175\ U^2+0.2558\cdot|U|+0.002$ [m/s]

These calibration equations provide accurate velocity estimates over a defined range, with a typical accuracy of ±1% of the reading and a minimum absolute error of ±0.01 m/s.

For practical implementation, we pre-defined the operational voltage range of the EMS sensors between **-1 V and +1 V**. This was done to ensure all measurements fall within the reliable and most accurate portion of the calibration curve. Given this, a simple approximation for converting voltage to velocity in the **X-direction** is to multiply the recorded voltage by **0.1023**, which is the dominant linear coefficient in the full calibration polynomial. This allows for a fast conversion in post-processing, particularly when high-accuracy second-order fitting is unnecessary.

As all EMF units are of the same model and calibrated under similar procedures, one representative calibration sheet (e.g., E661) can be adopted for conversion of all EMF data.

EMS calibration certificate

Enabling Delta Life

Type:	E30
Model:	Standard
Identification:	E661
S/N:	E661
Date:	20 April 2021
Water Temp.:	15.5 °C
Engineer:	C. van Nieuwenhuizen
Reviewer:	W. Taal
Generic formula's:	$\|V\| = -0.000188\ U^2 + 0.1023\ \|U\| + 0.002$ m/s Range: 1.0 m/s
	$\|V\| = -0.001175\ U^2 + 0.2558\ \|U\| + 0.002$ m/s Range: 2.5 m/s
Accuracy:	1 % of reading +/- 0.01 m/s
Calibration result:	passed

X-direction (PEMS output-0)				Y-direction (PEMS output-1)			
Vref	Ux	Vx	Error-X	Vref	Uy	Vy	Error-Y
(m/s)	(v)	(m/s)	(m/s)	(m/s)	(v)	(m/s)	(m/s)
-2.500	-10.238	-2.498	0.002	-2.501	-10.248	-2.500	0.001
-1.500	-6.059	-1.509	-0.009	-1.500	-6.068	-1.511	-0.011
-1.000	-9.995	-1.006	-0.006	-1.000	-10.007	-1.007	-0.007
-0.400	-3.832	-0.391	0.008	-0.400	-3.851	-0.393	0.006
-0.100	-0.857	-0.090	0.010	-0.100	-0.865	-0.090	0.009
0.000	0.000	-0.002	-0.002	0.000	0.000	0.002	0.002
0.100	0.880	0.092	-0.008	0.100	0.868	0.091	-0.010
0.400	3.858	0.394	-0.006	0.400	3.840	0.392	-0.008
1.000	10.017	1.008	0.008	1.000	10.024	1.009	0.008
1.501	6.042	1.505	0.004	1.501	6.075	1.513	0.012
2.501	10.298	2.512	0.010	2.501	10.313	2.515	0.014

Vref = velocity carriage Calibration Flume
Uxy = measured output signals PEMS ('voltage'mode)

Vxy = calculated velocities EMS
error-XY = Vxy - Vref

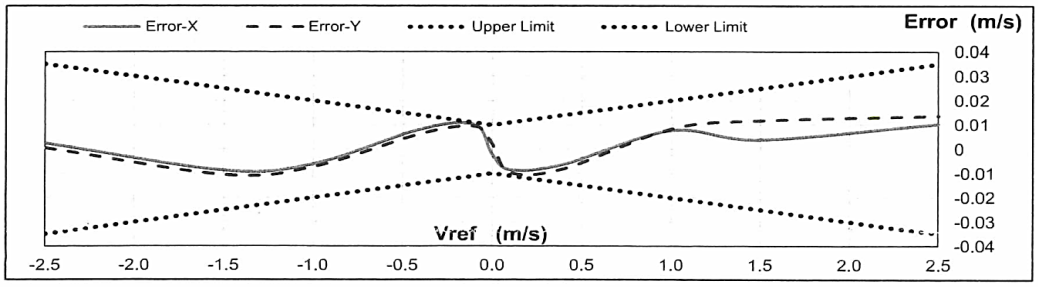

Remarks:

Used Equipment:

Signal:	*Device:*	*S/N:*	*ID-Deltares:*	*Manufacturer:*
output-0 and output-1	PEMS	100198	02.00.368	Deltares
Vref Ux Uy	NI 9205 (An.Inp.Module)	-	-	National Instruments
Complete Case DAQ	cDAQ-9191	-	-	National Instruments

Figure 18 - Deltares calibration certificate for Electromagnetic Flow Meter (called EMS in this document) unit E661 used in the physical modeling campaign.

B3. Pressure Sensors

Sensors 1 in each type (Kulite1 and Honey1) are at the bottom (lower part of the dike slope), while sensors 8 (Kulite8 and Honey8) are at the top (see Figure 6 and Figure 9 for details on the sensors' positioning).

During the flume tests, two types of piezoresistive pressure transducers—Kulite and Honeywell—were deployed along the 18° sloping of the dike body. Each sensor was mounted level with the slope surface, with Sensor 1 located at close to the toe of the dike (lowest vertical position) and Sensor 8 near the crest (highest vertical position). The exact vertical distance from the flume bottom to the center of each sensor was measured and recorded for accurate calibration.

The pressure sensors output voltages proportional to the absolute pressure exerted by the overlying water column. To calibrate these sensors, a series of static water levels were imposed in the flume. For each level, the corresponding sensor voltages were recorded and averaged. The effective water height above each sensor was then computed as the difference between the imposed still water level and the known vertical elevation of the sensor. Under hydrostatic assumptions, this vertical water column corresponds directly to the pressure head (in meters of water), allowing a direct empirical mapping between sensor voltage and pressure head.

It is assumed throughout the calibration that the atmospheric pressure remains constant across all calibration points. Therefore, any voltage offset due to barometric pressure is absorbed into the intercept of the calibration function. However, recognizing that atmospheric pressure and temperature can vary throughout dynamic tests, an auxiliary dataset is available for users who wish to compensate for such changes (see the second row dataset in the following table). This auxiliary set includes synchronized measurements from two pressure sensors—one fully submerged and another exposed to air—enabling dynamic correction for pressure drift caused by atmospheric or thermal fluctuations.

Table 18 - Calibration files for the pressure sensors

Num.	Date of Conduct	Test name	Description
1	04/April/2025	Main_Pressure_Sensors	Main calibration test for pressure sensors at the slope of the dike
2	08/May/2025	Pressure_diff_compensators	Calibration for two pressure sensors for compensating for the pressure difference due to temperature or atmospheric pressure change

Calibration Methodology Using a Linear Model

The methodology used for calibrating the pressure sensors closely follows the approach previously applied for wave gauge calibration. However, in this case, additional filtering steps were introduced to improve the robustness of the linear model. Specifically, data points corresponding to water levels below the center of the sensor were excluded, as they do not contribute meaningful hydrostatic pressure information. Furthermore, isolated outliers—data points lacking nearby neighbors in the voltage–pressure space—were identified and removed to prevent them from extremely influencing the calibration results.

The removed negative values and identified outliers are visually distinguished in Figure 19, with black and orange crosses, while the final calibration formulas for all pressure sensors are summarized in Table 19.

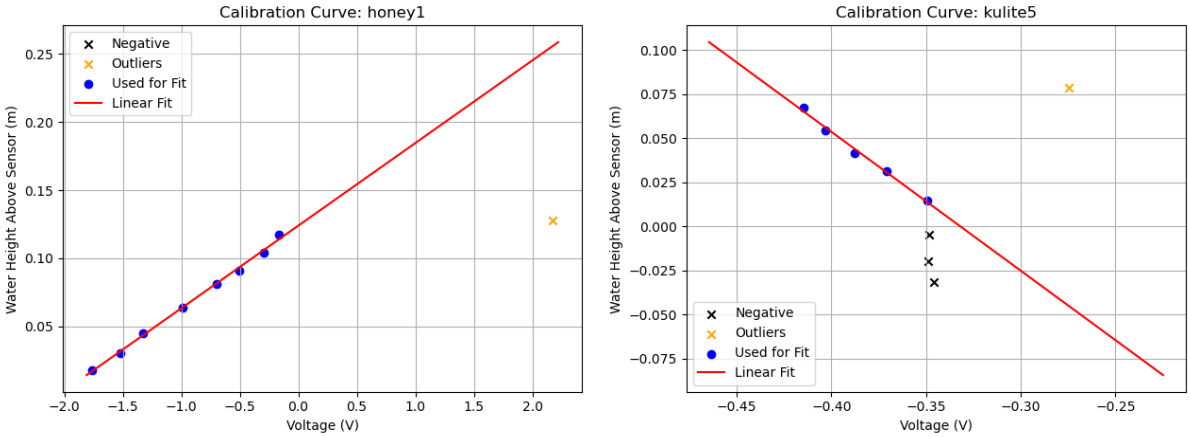

Figure 19 - Fitted models and calibration data as well as removed data for Honeywell 1 and kulite 5. The black crosses correspond to water levels for which this specific sensor was out of the water (negative water depth above the sensor, excluded from the fitting procedure). The yellow crosses are isolated outliers that were also discarded.

Table 19 - The final calibration formulas for all pressure sensors; The color indicate the reliability of the obtained calibration formula (red: unreliable; orange: questionable)

Num.	Test name	Calibration Formula
1	Main_Pressure _Sensors	kulite1_head(m) = -0.5242 + -0.7727 × voltage(V) kulite2_head(m) = -2.0256 + 1.4283 × voltage(V) kulite3_head(m) = -0.0729 + -0.9130 × voltage(V) kulite4_head(m) = -1.4949 + 1.3209 × voltage(V) kulite5_head(m) = -0.2615 + -0.7878 × voltage(V) kulite6_head(m) = -2.0062 + 1.0926 × voltage(V) kulite7_head(m) = -0.9978 + 1.3158 × voltage(V) kulite8_head(m) = -4.2501 + 3.1004 × voltage(V) honey1_head(m) = 0.1239 + 0.0607 × voltage(V) honey2_head(m) = 0.1143 + 0.0569 × voltage(V) honey3_head(m) = 0.0841 + -0.0151 × voltage(V) honey4_head(m) = 0.0934 + 0.0495 × voltage(V) honey5_head(m) = 0.0901 + 0.0809 × voltage(V) honey6_head(m) = 0.0726 + 0.0636 × voltage(V) honey7_head(m) = 0.0498 + 0.0802 × voltage(V) honey8_head(m) = -0.0380 + 0.1394 × voltage(V)

It is worth noting that while most sensors yielded well-fitted calibration models, the result for Honeywell 3 deviates from the expected behavior (highlighted with red font color in Table 19, see also Figure 20, left plot). Recalibration or further refinement of the input dataset, such as removing additional non-representative points, may be necessary. Additionally, it should be noted that because only a few points were available to perform the calibration at the highest sensors, Honeywell 8 and Kulite 8 (see right plot in Figure 20), the provided calibration formulas are likely less reliable than those of the other sensors.

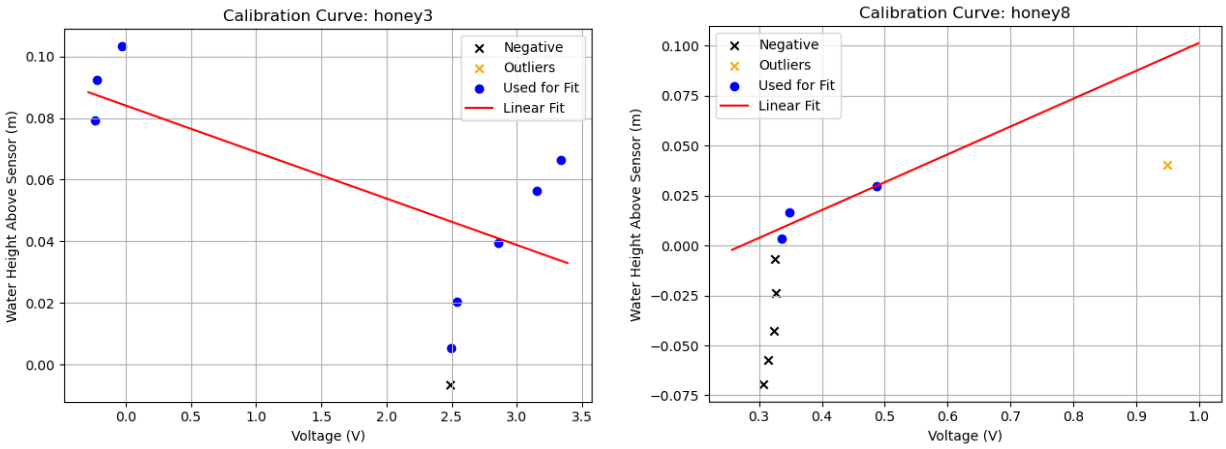

Figure 20 – Examples of unreliable calibration fits for the pressure sensors: (left) Honeywell 3 and (right) Honeywell 8.

B4. Ultrasonic (Microsonic) Sensors at Top of Dike

Two Ultrasonic sensors were installed at the crest of the dike to monitor overtopping water depth. Ultrasonic 1 was located near the seaward edge of the crest, while Ultrasonic 1 was positioned closer to the landward end of the slope. These sensors were calibrated to convert raw voltage/distance readings into water levels, providing direct measurements of the thickness of the water layer overtopping the dike during wave run-up events.

The calibration procedure followed the same methodology used for wave gauges in other parts of the flume. For each calibration step, mean voltage/distance readings were recorded with a series of fixed-height plywood plates positioned beneath the sensors. These known elevations provided reference distances for establishing the voltage-to-water-depth relationship. A linear model was then trained for each sensor to map voltage to water depth. The resulting calibration functions are presented in Table 21, and the fitted curves based on the calibration data are visualized in Figure 21. The calibrated values represent the vertical thickness of the overtopping water layer at the crest location of each Ultrasonic.

Table 20 – Calibration files for ultrasonic sensors

Num.	Date of Conduct	Test name	Description
1	08/April/2025	First_Mics_Calibration	Calibration set before starting the physical modelling
2	30/April/2025	Second_Mics_Calibration	Calibration set before removing the dike

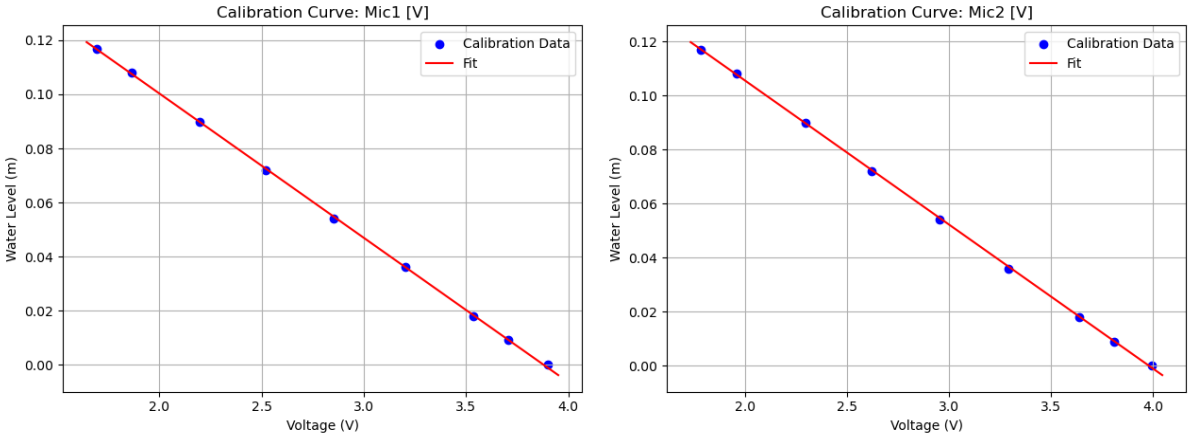

Figure 21 - Fitted models and calibration data for ultrasonic sensor MIC1 (left) and MIC2 (right).

Table 21 - The final calibration formulas for all Ultrasonic Sensors 1 and 2

Num.	Test name	Calibration Formula
1	First_Mics _Calibration	Mic1 [V]_level(m) = 0.2005 + -0.0512 × voltage(V) Mic2 [V]_level(m) = 0.2101 + -0.0522 × voltage(V)
2	Second_Mics _Calibration	Mic1 [V]_level(m) = 0.2071 + -0.0534 × voltage(V) Mic2 [V]_level(m) = 0.2122 + -0.0533 × voltage(V)

B5. Wave Gauge and the Ultrasonic Sensor in the Overtopping Tank

To accurately quantify the water level measured by both the wave gauge and ultrasonic sensor installed in the overtopping tank setup, a calibration process was carried out. This process involved gradually filling the overtopping tank with water to predefined levels, while recording the sensor output voltages using two types of instruments: traditional resistive wave gauges (WG15) and a non-contact ultrasonic sensor (MIC3).

For each of these sensors, the mean voltage was computed at each water level step. These (voltage, water level) pairs formed the training data used to derive calibration models. Similar to the previous approaches, a linear regression model was fitted to the data for each sensor (see examples in Figure 22) resulting in a formula that relates voltage to water level in meters (Table 23).

Table 22 – Calibration files for the WG inside the overtopping tank

Num.	Date of Conduct	Test name	Description
1	08/April/2025	First_Overtopping _Tank_Calibration	First overtopping calibration dataset
2	02/May/2025	Second_Overtopping _Tank_Calibration	Second overtopping calibration dataset

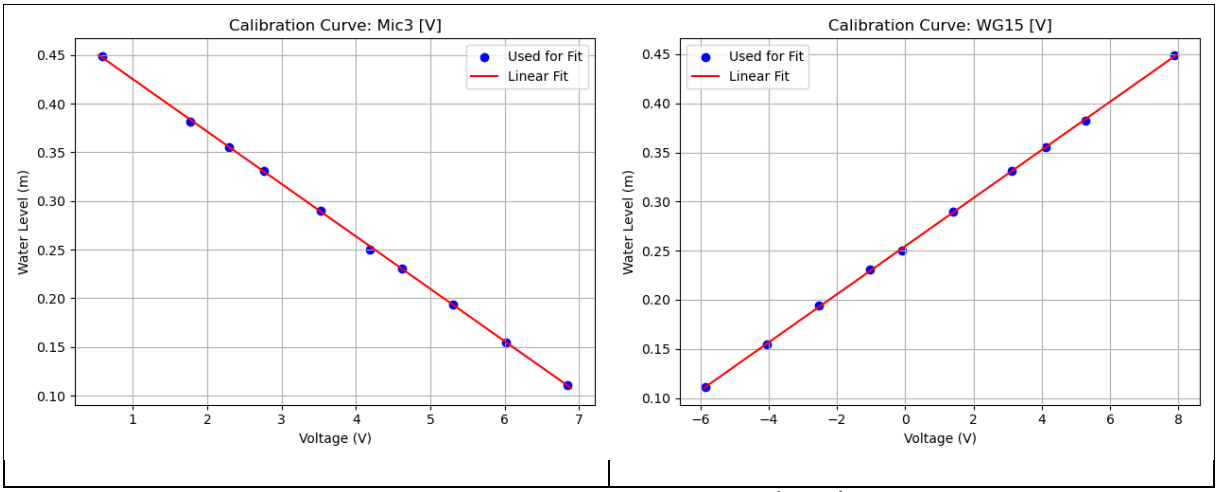

Figure 22 - fitted models and calibration data for ultrasonic sensor 3 (MIC3) and Wave Gauge 15, located in the overtopping tank.

Table 23 - The final calibration formulas for all Ultrasonic Sensors and the wave gauge

Num.	Test name	Calibration Formula
1	First_Overtopping _Tank_Calibration	WG15 [V]_level(m) = 0.2561 + 0.0240 × voltage(V) Mic3 [V]_level(m) = 0.4767 + -0.0528 × voltage(V)
2	Second_Overtopping _Tank_Calibration	WG15 [V]_level(m) = 0.2546 + 0.0245 × voltage(V) Mic3 [V]_level(m) = 0.4792 + -0.0539 × voltage(V)